Biophys Rep 2025, 11(X):1–29
https://doi.org/10.52601/bpr.2025.240073 https://cstr.cn/32402.14.bpr.2025.240073
Biophysics Reports

REIVEW

Interactions between membrane proteins and lipid membrane revealed by cryoEM

Sixian He[1#], Yun Han[1#], Xinying Liu[1], Yusong R. Guo[1] ✉

[1] Department of Biochemistry and Molecular Biology, School of Basic Medicine, Tongji Medical College, Huazhong University of Science and Technology, Wuhan 430030, China

Received: 31 December 2024 / Accepted: 31 March 2025

Abstract Membrane proteins and membrane lipids are essential partners in various biological processes, and elucidating their structures in a natural membrane environment is crucial for enhancing our understanding of their intricate interactions. However, resolving high-resolution structures of lipids and membrane proteins under physiological conditions presents considerable challenges due to limitations in experimental techniques and instrumentation, leaving these interactions inadequately understood and necessitating further investigation. In this review, we summarize current sample preparation methods and tools for studying lipid-membrane protein interactions using cryo-electron microscopy (cryo-EM), including nanodiscs, styrene-maleic acid copolymers, liposomes, and *in situ* analyses. We also highlight several up-to-date examples of high-resolution lipid-membrane protein complexes that reveal how lipids influence the functionality of membrane proteins, featuring the innovative methodologies employed. Additionally, we provide a concise overview of the steps involved in cryo-EM analysis of membrane proteins and summarize recent advancements in deep learning techniques for model construction. We discuss how the intersection of artificial intelligence and structural biology offers a fertile ground for breaking through current technological barriers, promising to unravel the complexities of molecular dynamics and providing a holistic view of biomolecular interactions.

Keywords Membrane protein, Protein–lipid interaction, Cryo-EM, Cryo-ET, *In situ*

INTRODUCTION

Biological membranes are very sophisticated. As the two most important components of the cell membrane, lipids and proteins are closely related. LIPID MAPS (LIPID Metabolites and Pathways Strategy) Consortium developed a comprehensive classification system for lipids based on their chemical composition: fatty acyls, glycerolipids, glycerophospholipids, sphingolipids, saccharolipids, polyketides, sterol lipids and prenol lipids (Fahy *et al*. 2005). In addition to this classification scheme, lipids can also be divided into three main subcategories based on their interactions with membrane proteins transmembrane domains (TMDs)-bulk lipids, annular lipids, and nonannular lipids. Bulk lipids do not directly interact with membrane protein but they could impact membrane protein geometry (Polley *et al*. 2017). Hence they are involved in various signaling pathways including JAK/STAT (Blouin *et al*. 2016) and Wnt/β-Catenin (Özhan *et al*. 2013; Sezgin *et al*. 2017) and have an impact on protein transport (Brown and Rose 1992; Lajoie and Nabi 2010) and dynamics (Lin *et al*. 2017; Tisza *et al*. 2016). Both annular lipids and nonannular lipids directly interact with membrane proteins. Annular lipids, known as "boundary lipids", form a ring around the TMDs of proteins in a non-specific way (Jost *et al*. 1973). On the contrary, nonannular lipids specifically interact with proteins and regulate protein conformations (Anderluh *et al*.

[#] Sixian He and Yun Han contributed equally to this work.

✉ Correspondence: yrguo@hust.edu.cn (Y. R. Guo)

2017; Marsh 2007; Westerlund *et al*. 2020; Yen *et al*. 2018) and functions (Chavent *et al*. 2018; Coskun *et al*. 2011). Overall, lipid–protein interactions are engaged in numerous biological processes, for example, the folding of membrane proteins (Dowhan *et al*. 2019), maintenance of the optimal activity of integral proteins (Mileykovskaya and Dowhan, 2014) and membrane bending (Pang *et al*. 2023).

Besides, lipids themselves can act as a substrate for protein during transport (de Saint-Jean *et al*. 2011; Ikonen and Zhou 2021) or the first and second messengers in signal transduction and molecular recognition processes (Meyer zu Heringdorf and Jakobs 2007), for instance, sensory transduction (Hilgemann *et al*. 2001; Suh and Hille 2005) including heat, pain (Chuang *et al*. 2001), bitter and sweet (Liu and Liman 2003), cell survival pathway (Brunet *et al*. 2001) and T lymphocyte signaling (Ueda *et al*. 1995). Moreover, lipid metabolism, which is precisely controlled, plays a crucial role in various functions within our body, including energy storage and hormone regulation. Lipid metabolism abnormalities lead to various diseases such as neurodegenerative diseases (Cheng *et al*. 2011; Fabelo *et al*. 2014; Phillips *et al*. 2020; Tong *et al*. 2015), coronary artery disease, hyperlipidemia (Natesan and Kim 2021), and insulin resistance (Azhar 2010). Numerous studies indicate that changes in membrane lipid composition, influenced by lipid metabolism, affect the distribution of membrane proteins, leading to diseases. In Niemann-Pick type C (NPC) disease, lipid accumulation altered the distribution of NPC1 (a cholesterol-sensing protein that is defective in NPC disease) (Puri *et al*. 1999). Also, membrane protein lipidation is regulated by lipid metabolism and plays a role in cancer-related pathways. For example, glucose transporter 1 (GLUT1) S-acylation promotes glioblastoma glycolysis and tumorigenesis (Zhang *et al*. 2021). The binding of palmitoleoylated WNT protein to the Frizzled receptor and low-density lipoprotein-related receptors 5/6 (LRP5/6) contributes to cell survival (Flanagan *et al*. 2022; Mo *et al*. 2013).

Thus, exploring the interplay of membrane lipids and membrane proteins, as well as their interactive regulatory mechanisms, is of great significance. Although X-ray crystallography and cryo-electron microscopy (cryo-EM) single-particle analysis (SPA) are widely used tools to gain high-resolution structural information of membrane proteins, traditional solubilization and purification processes separate membrane proteins from relevant lipids, especially bulk lipids. Only for lipids that are tightly bound, for example, in the case of K_{2P}10.1 (TRAAK, TWIK-RElated Arachidonic Acid activated K^+ channel), the little amount of lipids could be co-purified with the target membrane protein for mechanistic investigations. It is thus crucial to engage appropriate approaches to enhance our understanding of membrane proteins and their associated lipids (Dong *et al*. 2015).

In cellular environments, the phospholipid composition is essential for maintaining the stability of membrane proteins and plays a significant role in mediating their activity. Conversely, membrane proteins can also influence the distribution of phospholipids and the curvature of the membrane. This review gives a comprehensive summary of the current methods and tools for studying lipid-membrane protein interaction, which may bring the ultimate goal of obtaining the entire structure of the lipid-membrane protein complex in their native membrane environments one step closer to reality. By advancing these methods, scientists could better uncover the pathological mechanism underlying lipid metabolism dysfunction. Furthermore, these technologies could be utilized to illustrate how lipids affect protein–drug interactions and assist in the development of drugs that target both lipids and membrane proteins or protein lipidation.

MEMBRANE PROTEIN SAMPLES FOR STRUCTURAL STUDIES USING CRYO-EM

With the continuous advancement of electron microscopy, it has become possible to obtain high-resolution structures of membrane proteins. Sample preparation constitutes a pivotal step that enables researchers to elucidate the three-dimensional structure of membrane proteins with near-atomic level resolution. In cellular environments, the phospholipid composition is essential for maintaining the stability of membrane proteins and plays a significant role in mediating their activity. Conversely, membrane proteins can also influence the distribution of phospholipids and the curvature of the membrane. New methods are being developed to gather structural information on membrane proteins, especially in their native environment, to investigate the interactions between the phospholipid environment and membrane proteins.

Nanodisc

Detergents, while effective in extracting proteins from cells to simplify downstream analysis, can disrupt the tertiary structure of membrane proteins, reducing stability and causing unfolding (Padmanabha Das *et al*. 2020). For samples used directly for structural analysis,

detergents such as OGNG, and LMNG have been extensively utilized in the successful determination of a broad array of membrane protein structures (Lee 2022).While for nanodiscs, detergents like DDM, C12E10, GDN, and CHAPS can stabilize membrane proteins, promoting the formation of nanodiscs (Fig. 1).

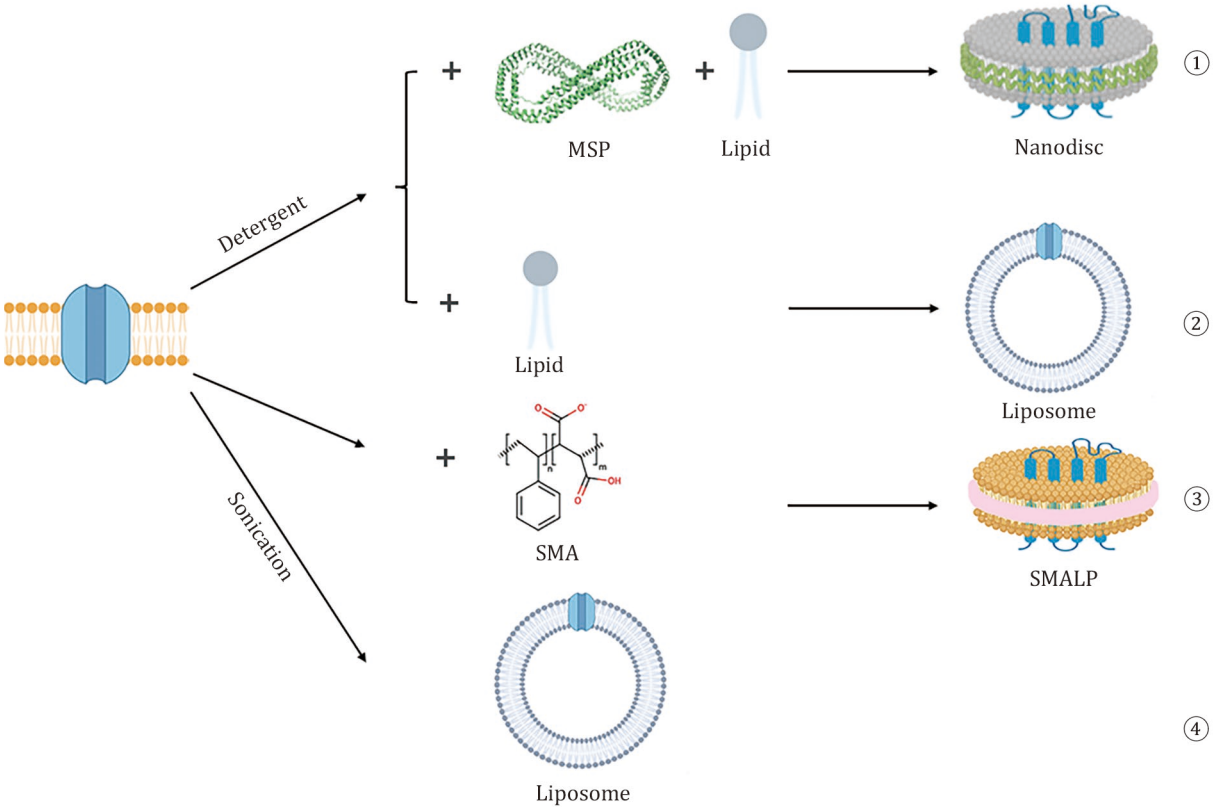

Fig. 1 Schematic representation of methods for membrane protein sample preparation. ① Nanodisc. Membrane proteins are purified from cell membranes using detergents, followed by the addition of MSP (PDB ID 1AV1) and phospholipids to form nanodiscs. Detergents commonly used for the preparation of nanodiscs and proteoliposomes are listed (Lin *et al*. 2019; Lige and Wang 2020; Schmidpeter and Nimigean 2021; Skarda *et al*. 2021; Tonggu and Wang 2022; Yang *et al*. 2022; Han *et al*. 2024). ② Proteoliposome. Membrane proteins are extracted from cell membranes using a detergent, followed by the addition of phospholipids to create a homogeneous solution. Finally, the detergent is removed to form the proteoliposome. ③ SMALP. SMA is added to the cell lysate, and the SMA polymer surrounds a small portion of the membrane. This process enables the extraction of membrane proteins along with their associated phospholipids, resulting in the formation of SMALPs. ④ Native liposome. By sonication, the cells are made to form native liposomes. The native liposomes could be obtained by three methods: sonicating cells, inducing the formation of NMVs from the plasma membrane, and collecting exosomes in cell culture medium (Fu and MacKinnon 2024)

Nanodiscs are formed by amphipathic helical proteins derived from Apolipoprotein A- I (ApoA-I), which stabilize phospholipids into disc-shaped bilayers (Bayburt *et al*. 2002) (Fig. 1). Nanodiscs provide a more stable environment for membrane proteins, mimicking biological membranes and maintaining native conformation and activity (Rouck *et al*. 2017). They are tunable in size, uniform, and long-lasting, enhancing protein contrast in electron microscopy for high-resolution structural analysis (Denisov and Sligar 2017; Hein *et al*. 2014). Generally speaking, for the preparation of nanodiscs, the detergents were gradually removed from the purified protein sample by dialysis or gel filtration, then the membrane scaffolding proteins (MSPs) and the phospholipids were added to facilitate the self-assembly of the nanodiscs. The specific methods for preparing nanodiscs could be found in recent reviews (Denisov and Sligar 2016; Pettersen *et al*. 2023; Strickland *et al*. 2021).

Due to factors such as the fluidity of phospholipids, studying the interaction between lipids and membrane

proteins is quite challenging (Denisov and Sligar, 2024). A novel method termed "lipid titration" has been developed for force-resolved structural studies using nanodiscs (Han *et al*. 2024). This mechanical force simulation approach focuses on the structural dynamics of membrane proteins and has been instrumental in understanding the underlying mechanisms of force-induced gating in the OSCA channel and the formation of proteo-lipidic pores for ion conduction. Two distinct scaffold proteins, MSP1E3 and MSP2N2, were employed in the preparation of nanodiscs to facilitate the visualization of lipid interactions with Ca^{2+}-bound fungal nhTMEM16 at the closed groove (Feng *et al*. 2024). This methodological approach underscores the versatility of nanodiscs in studying protein-lipid interactions and the influence of scaffold proteins on the conformational landscape of membrane proteins, the use of different MSPs allows for the exploration of the functional expression of membrane proteins in different environments. The different effects of MSP1E3 and MSP2N2 on the conformation of membrane proteins during the formation of nanodiscs also provide a tool for studying the functional diversity and regulatory mechanisms of membrane proteins. However, there are some limitations to this method. The size of nanodiscs may affect the conformation of the encapsulated membrane proteins, as the diameter of lipid nanodiscs is mostly between 8–20 nm, which is smaller than many membrane proteins that need to be encapsulated (Zhao 2024). Within nanodiscs, lipids and protein molecules frequently encounter the belt of the membrane scaffold protein, which affects the dynamics and structure of the protein molecules. Due to the limited size of nanodiscs and the presence of the membrane scaffold protein, the physical and chemical properties of the lipid bilayer, such as lipid packing, fluidity, and rigidity, are affected (Real Hernandez and Levental 2023). In addition, artificial lipid components do not fully mimic the complexity and diversity of natural membranes (Inagaki *et al*. 2013). Since membrane protein-lipid interactions are critical for maintaining protein structure and function, the use of artificial lipids may cause structural distortions and lead to misleading conclusions (Wang and Tieleman 2024).

SMALP

In recent years, Styrene-maleic acid (SMA) as well as new synthetic copolymers based on SMA and its derivatives have been reported to be effective carriers of membrane protein for cryo-EM. SMA, an amphiphilic polymer composed of a hydrophobic styrene moiety and a hydrophilic maleic acid, represents itself in aggregated form and tries to insert the hydrophobic styrene moiety into the acyl chain of phospholipids. When the polymer has encircled a tiny piece of the membrane, it is pulled out, resulting in styrene-maleic acid lipid particles (SMALPs) (Karanth *et al*. 2024; Orekhov *et al*. 2022) (Fig. 1). The preparation method for SMALPs is still being improved (Broadbent *et al*. 2022; Glukhov *et al*. 2024; Sawczyc *et al*. 2023; Ullrich *et al*. 2024). These extraction techniques eliminate the need for detergents while preserving the interaction between lipids and membrane proteins (Ayub *et al*. 2024). In contrast to detergents, it was reported that membrane protein extraction using SMA is more beneficial to preserving the stability of membrane proteins (Zhou *et al*. 2023). The method of generating SMALP-like discs is suitable for using cryo-EM to investigate the lipid-GPCR proteins interactions, understand the effect of lipids on receptor function during GPCR protein activation (Ayub *et al*. 2024), and explore the structural dynamics of the potassium channel membrane protein KCNQ1 voltage-sensing domain (Scheyer *et al*. 2023). In recent years, high-resolution structures obtained by cryo-EM of SMALPs, formed by isolating multiple membrane proteins using polymers, have been conducive to understanding membrane protein–lipid interactions (Krishnarjuna and Ramamoorthy 2022). A density map resolution of 3.2 Å was obtained for the multidrug efflux transporter AcrB, which was isolated using SMA (Qiu *et al*. 2018). The high-resolution structural folding of EspP (containing a 12-stranded β-barrel and a canonical β-signal) in complex with BamA, isolated using SMA, has been determined by cryo-EM (Doyle *et al*. 2022). By identifying the β-signal of EspP, BamA is able to catalyze the assembly of EspP in the outer cell membrane. In SMALPs, a continuously open BamA β-barrel and multiple hybrid-barrel substrates were revealed during the folding process of EspP. A change in the membrane around the folding intermediate was first detected, and the change could also affect the folding of EspP.

Additionally, this method is valuable for developing more accurate drug-screening platforms (Oates and Watts 2011) and enhancing drug delivery (Hosokawa *et al*. 2024; Mu *et al*. 2024). However, the method requires high membrane protein concentration and solubility (Broadbent *et al*. 2022; Wang *et al*. 2024b). Proteins may dissolve in lipids due to a phase transition, although this process may occur more slowly at a temperature of 4°C (Broadbent *et al*. 2022; Kopf *et al*. 2020). The structural stability of polymer–lipid–protein particles derived from various SMA variants may be partially or completely modified (Hoang Trinh *et al*. 2023). It is important to note that the method has limitations in achieving high-resolution structures.

Liposome

Liposomes are spherical or multilayered spherical vesicles formed from the self-assembly of diacyl-chain phospholipids (lipid bilayer) in aqueous solutions (Nsairat *et al*. 2022). The approach of embedding membrane proteins in liposomes has been widely employed for the functional and structural investigation of membrane proteins. The necessity for reconstitution arises because many membrane proteins express their full activity only when correctly oriented and inserted in a lipid bilayer (Rigaud and Lévy 2003).

To reconstitute membrane proteins into liposomes, membrane proteins are purified and solubilized in detergents. Then the protein/detergent mixture is mixed with the lipid/detergent mixture to form a homogenous solution. Finally, the homogenous solution was removed from detergents to generate proteoliposomes (Wang and Tonggu 2015; Yao *et al*. 2020) (Fig. 1). Artificial lipid components also have been widely used for reconstituted liposomes, which allows for a controlled lipid composition while maintaining membrane protein function (Herbert *et al*. 2021.). It is possible to influence the physical properties of membranes and thus regulate the conformation, activity, and localization of membrane proteins by artificially altering, for example, the composition of lipids (Casares *et al*. 2019; Fratti 2021, Pozza *et al*. 2022).

Proteoliposomes partially recover the intracellular electrochemical gradients and membrane curvature of membrane proteins, which is beneficial to investigate the impact of the transmembrane gradient of ions or other substrates on the structure and function of the target proteins, such as the voltage-gated ion channels and proton-driven transporters (Yao *et al*. 2020). In addition, the method can also be utilized to investigate the biophysical principles and mechanisms underlying the tension-dependent activation of the mechanosensitive ion channel Piezo (Haselwandter *et al*. 2022; Tong *et al*. 2015; Yang *et al*. 2022). Notwithstanding these advances, the reconstitution procedure is difficult in some cases, especially if the membrane protein requires stabilization in a low critical micelle concentration detergent. Moreover, lipids used in the reconstitution will not likely replicate the composition of a cell membrane when the membrane composition is unknown. Of equal importance, the detergent extraction step prior to reconstitution will most assuredly result in the loss of cofactors and associated proteins, which may be weakly bound yet essential for normal biological function.

To solve these problems, methods of extracting endogenous vesicles have been proposed, including the isolation of fragments of native cell membranes in the form of small vesicles and the extraction of functional synaptic vesicles from mouse brains (Wang *et al*. 2024a). These methods don't remove a protein from the membrane, which helps stabilize membrane protein and preserve a local environment for the protein that is closer to its natural environment in the cell. Using this method, it is also possible to discover associated molecular partners such as small molecules, lipids, and other proteins that normally dissociate under traditional purification methods (Tao *et al*. 2023).

In situ

While the sample preparation approaches mentioned above could help characterize membrane protein in a near-native lipid environment, the topology of the membrane is disrupted hence abolishing membrane curvature (Yao *et al*. 2020). In recent years, the application of cryo-electron tomography (cryo-ET) technology has provided a powerful tool for studying the natural structure of membrane proteins in the cellular environment and their interactions with the cell membrane at their original location (*in situ*), which is helpful to reserve this characteristic (Keller and Fernández-Busnadiego 2024). Additionally, it is capable of capturing the distribution and conformational changes of proteins under near-physiological conditions with nanoscale resolution (Dutta and Acharya 2024). However, cryo-ET currently faces several limitations. It is primarily suitable for larger membrane protein complexes or highly abundant membrane proteins. Compared to single-particle analysis (SPA), for smaller membrane proteins, the technique struggles to accurately localize protein particles due to their lower contrast (Ching and Maufront 2024; Yan 2025).

The selection of suitable biological samples for *in situ* structural studies, including organelles, cells, and tissues, is of great importance (Keller and Fernández-Busnadiego 2024). For thicker samples, thin slices are prepared using a cryogenic focused ion beam (cryo-FIB) representing a state-of-the-art methodology for the preparation of samples for transmission electron microscopy (TEM). This technique allows for the precise cutting and processing of materials at cryogenic temperatures, resulting in the production of ultra-thin slices of samples (commonly referred to as "lamellae") that can be imaged and analyzed at high resolution in the TEM. Thin sections prepared by cryo-FIB ensure that the electron beam can effectively penetrate the sample (Long *et al*. 2022). The *in situ* structure of membrane proteins could be analyzed by acquiring a series of tilt-angle two-dimensional projection images. To enhance image quality, denoising and image segmenta-

tion techniques are often employed to identify and select specific structures within the sample. Subtomogram averaging (STA) is then performed on these selected, structurally similar particles to enhance the signal-to-noise ratio, thereby significantly improving the resolution of the structures (Sexton *et al*. 2022; Zhu *et al*. 2022).

Cellular *in situ* structural studies have been extensively employed to investigate the structural characteristics of channels, receptors, and transporter proteins on diverse cell membranes (Pöge *et al*. 2021; Zila *et al*. 2021; You *et al*. 2023; Dahmane *et al*. 2022; Tran *et al*. 2021; Zhao *et al*. 2022; Klein *et al*. 2023, 2020). Cryo-ET has been utilized to identify previously unreported interactions between vesicular (H^+)-ATPase (V-ATPase) and synaptophysin within synaptic vesicles (SVs) (Wang *et al*. 2024a). This method, when combined with liposome structural analysis and *in situ* structural analysis, enables a more comprehensive observation of the interactions between membrane proteins and surrounding lipids under physiological conditions, providing valuable insights into the molecular mechanisms underlying neurotransmitter release and its regulation, as well as the organization of membrane proteins and lipids within the synaptic vesicle environment (Xu *et al*. 2024a).

Despite its considerable potential in membrane protein research, cellular *in situ* structural studies are confronted with a number of challenges. The generation of sub-nanometre resolution structures, for instance, remains a relatively uncommon occurrence (Watson and Bartesaghi 2024). The processing of *in situ* structural studies data necessitates the utilization of sophisticated computational techniques and high-performance computing resources. Besides, cryo-FIB, as a technique used to prepare ultra-thin sections for high-resolution electron microscopy imaging is typically both time-consuming and laborious.

ADVANCED UNDERSTANDINGS IN THE STRUCTURES AND FUNCTIONS OF MEMBRANE PROTEINS

Membrane proteins interact with and influence their surrounding lipid environment, thus playing crucial roles in numerous cellular physiological processes, including signaling, membrane transport, and energy conversion. Advancements in technology have led to significant progress in our understanding of the structure and function of membrane proteins, as well as the interactions between membrane proteins and their lipid environment through the use of cryo-EM.

OSCA channels

OSCA1.2 is a calcium ion channel found in plants and is a member of the mechanosensitive ion channel family (Murthy *et al*. 2018). In a hyper-osmotic environment, the influx of calcium ions is facilitated, playing a crucial role in the plant's perception of osmotic pressure. The high-resolution cryo-EM structure of OSCA1.2 in its closed state has been resolved, revealing a homodimer with each subunit containing 11 transmembrane helices (Liu *et al*. 2018). The dimer exhibited non-centrosymmetry and formed a V-shaped cavity between the transmembrane domains of the two monomers (Fig. 2A). This cavity opened to the extracellular side and was isolated from the cytoplasm. The molecular dynamics model of OSCA1.2's interactions with the phospholipid bilayer suggested that lipids could stabilize the assembly within the dimer's V-shaped cleft (Jojoa-Cruz *et al*. 2018). It was hypothesized that membrane tension might facilitate the gating process of the channel by influencing lipid occupancy in this region. However, lipid density was not detected in the structure of OSCA1.2 purified using detergent.

To investigate the correlation between the gating mechanism of OSCA and the lipid content in the V cavity, OSCA1.2 was reconstituted into nanodiscs at three different ratios of MSP to lipid and analyzed using cryo-EM (Han *et al*. 2024). As the lipid content in the nanodiscs decreased, leading to increased membrane tension, the degree of contraction of OSCA1.2 also increased. The OSCA family members OSCA3.1 and OSCA1.1 exhibited a similar trend. In the contracted OSCA structures, a significant widening of the membrane-side opening was observed. However, it is currently not possible to determine whether the channel is open due to a distinctly dilated pore.

To further confirm whether changes in local curvature can activate OSCA, the activation state of OSCA was studied using proteoliposomes of small diameters ($d \leq$ 40 nm). In the liposome structure of OSCA1.2, the protein exhibited two orientations: inside-out and inside-in. The inside-out structure resembled the closed state, as shown in the nanodisc structure mentioned above, whereas the inside-in structure featured a belt of membrane density that had been inserted into the gap and had extended along the pore, effectively sealing the lateral opening of OSCA. It was named the proteo-lipidic pore (Fig. 2B). A mechanical-coupling model has been proposed, suggesting that as membrane tension increases, lipids in the OSCA gap are continuously pulled out, thereby disrupting the stability of the helices bound to the lipids in OSCA. In order to maintain stability, the spiral rotation causes the gap to narrow, which

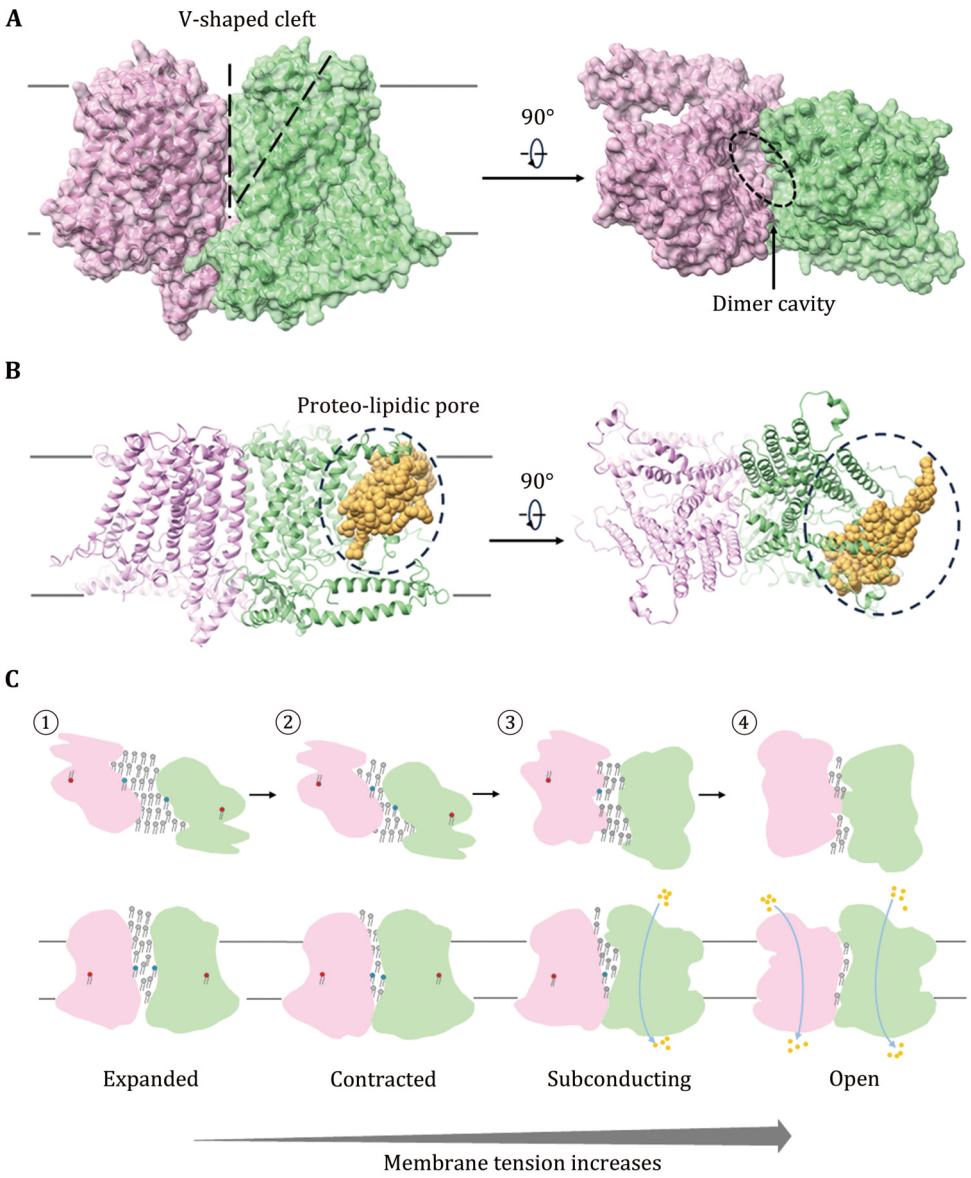

Fig. 2 Phospholipids are involved in the opening and closing of OSCA channels. **A** Overall dimeric structure of AtOSCA1.2 (PDB ID 6IJZ) in its closed state. A side view of the V-shaped cleft and an extracellular view of the dimer cavity. The model of OSCA1.2 is shown as surface. **B** The lateral and top views of the proteo-lipidic pore of the liposome-embedded OSCA1.2 (PDB ID 8XAJ) are shown as a cartoon. OSCA1.2 is shown in light pink and light green, while the lipids are shown in yellow. **C** ①–④, the activation pathway of the OSCA channel is shown in the top view (upper panel) and side view (lower panel). Under membrane tension, cleft lipids are continuously pulled out, causing the cleft to narrow. The OSCA channel transitions from the Expanded state ① to the Contracted state ②. As membrane tension increases, the tightly bound 'interlocking' lipids and the pore exit lipids on each subunit of the OSCA are pulled out independently. This process enables the OSCA subunit to form a proteo-lipidic ion pathway, referred to as the Subconducting state ③. The complete opening of the OSCA dimer results in the Open state ④. The colours of the two subunits are light pink and light green, respectively. The cleft lipids, 'interlocking' lipids and pore exit lipids are shown in gray, blue and red, respectively. Ions are indicated by yellow dots and permeation pathways are indicated by blue arrows. Adapted from reference (Han *et al*. 2024)

could lead to the opening of the channel (Fig. 2C). Utilizing liposomes in cryo-EM research has the potential to enhance our understanding of the conformational switching and mechanisms of mechanosensitive channels.

Piezo channels

The Piezo channel family, including Piezo1 and Piezo2 in mammals, are evolutionarily conserved and functionally diverse mechanosensitive cation channels, which

mediate key physiological and pathophysiological processes. The cryo-EM structure of recombinant mouse Piezo1 in the detergent micelle has been determined, revealing a three-bladed, propeller-like homotrimeric architecture with a core ion-conducting pore module topped with an extracellular cap domain (Guo and MacKinnon 2017; Saotome *et al*. 2018; Zhao *et al*. 2018) (Fig. 3A). The three blades are composed of transmembrane helices and do not lie in a plane in the closed conformation, which could induce the lipid bilayer to curve between the arms (Guo and MacKinnon 2017; Zhao *et al*. 2018). The structure of mouse Piezo2 is similar to mouse Piezo1 (Wang *et al*. 2019). To investigate the mechanism by which Piezo converts external mechanical stimuli into electrochemical signals, a membrane dome mechanism has been proposed, in which the membrane flattens upon the opening of the channel (Fig. 3A).

The detergent environment makes it challenging to establish a state under tension, which prevents the observation of Piezo flattening. The reconstruction of membrane proteins into liposomes enables the exploration of conformational changes in Piezo1. To confirm the reversible conformational change of Piezo1 flattening in response to membrane tension, the varying curvature of Piezo1 in a phospholipid environment was investigated quantitatively using cryo-EM and high-speed atomic force microscopy (HS-AFM) (Lin *et al*. 2019). Both methods demonstrated that Piezo1 could deform its shape towards a planar structure, which could explain how lateral membrane tension gates the Piezo channel. To further explore the structural details of the flattened Piezo1, the flattened structure of Piezo1 within the liposome was determined at medium resolution using cryo-EM (Yang *et al*. 2022). The pores of the flat Piezo1 channels appeared to be slightly expanded compared to those of the curved Piezo1 channel, and three blades underwent a downward motion to become totally co-planar. However, it is unclear whether Piezo1 is open under this condition due to the resolution limitations of the pore region.

There is still little mention in the aforementioned research of how Piezo interacts with its residing lipid membrane. Theoretical calculations and simulations showed that starting from the membrane dome Piezo can form a larger membrane footprint (Haselwandter and MacKinnon 2018) on the membrane region outside the dome (Haselwandter *et al*. 2022) (Fig. 3B). The

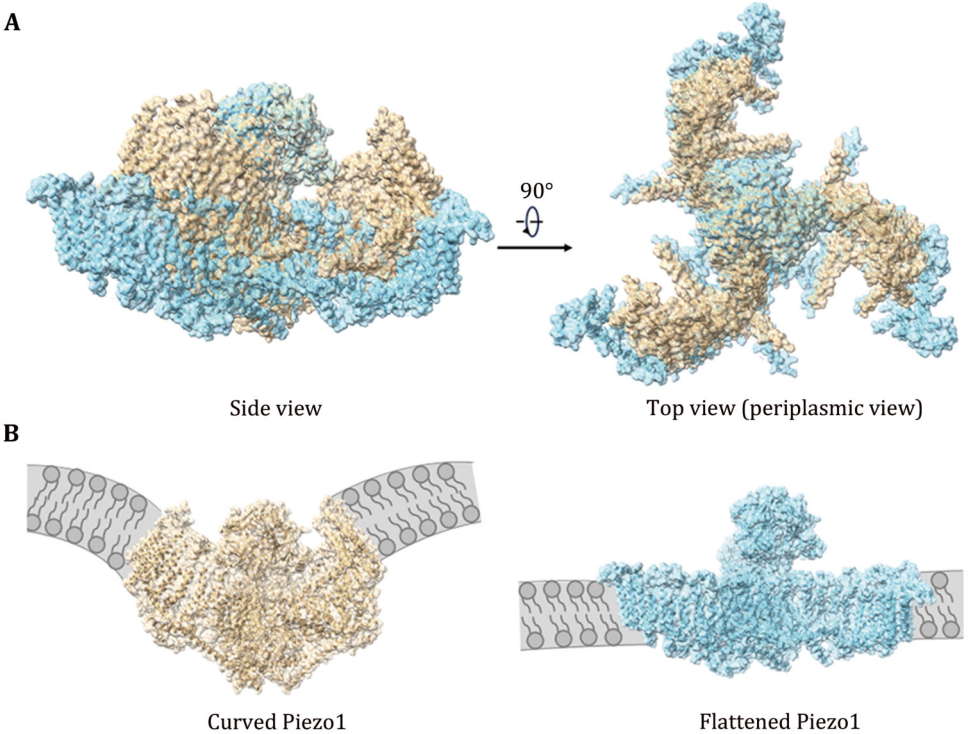

Fig. 3 Curved and Flattened States of the Piezo1 Channel. **A** The alignment of the curved (PDB ID 7WLT) and flattened (PDB ID 7WLU) liposome-embedded Piezo1 structures are shown in the side and top views. **B** Schematic representation of the hypothesized effects of the curved and flattened states of Piezo1 channels on membrane curvature. The curved and flattened forms of Piezo1 are shown as the surface. The curved Piezo1 is shown in yellow cream, the flattened Piezo1 in sky blue and the membrane in gray

shape of the membrane footprint is influenced by several key factors: the basic shape of the Piezo dome (curvature), the bending modulus of the membrane (stiffness), and the tension applied to the Piezo-membrane system. To experimentally measure the shape of the membrane containing Piezo without averaging out useful information, seven Piezo vesicles of varying radii were analyzed using cryo-ET (Haselwandter *et al*. 2022). The tomograms confirmed that these channels were predominantly reconstituted with their extracellular surfaces oriented toward the interior of the vesicle. In smaller vesicles, the Piezo dome was more curved, while in larger vesicles, it appeared flatter (Lin *et al*. 2019). The Piezo dome shapes derived from the minimization of the Helfrich energy equation, a physical principle that governs the shape of free membranes outside the Piezo dome, closely approximate the observed shapes of these domes. In the cases above, techniques for reconstructing liposome samples and cryo-ET were used to gain a deeper understanding of the interaction between Piezo and lipid membranes. Through the membrane footprints, Piezo and the free membrane interact with each other, affecting each other's distribution and Piezo's gating properties on the membrane.

To elucidate the Piezo-membrane interaction with more physiological relevance, the mechanical properties of Piezo need to be further studied *in situ* in different types of tissue cells, or even different membrane regions within the same cell, which exhibit varying mechanical properties of the membrane due to varying lipid compositions. In addition, the cytoskeleton divides the cell membrane into regions of varying sizes, which can subsequently alter the shape and size of the Piezo membrane footprint, thereby influencing the Piezo gating properties. Future studies of Piezo in the cellular environment using cryo-ET are expected to shed more light on the pathogenesis by gain- or loss-of-function mutations of Piezo, to facilitate the development of Piezo-specific drugs for treating conditions associated with Piezo abnormalities.

SPFH family

The SPFH (Stomatin, Prohibitin, Flotillin and HflK/C) family comprises a class of membrane proteins localized in various biological membrane systems (Browman *et al*. 2007; Lapatsina *et al*. 2012; Tavernarakis *et al*. 1999; Yokoyama and Matsui 2020). These proteins play crucial roles in maintaining the stability and functionality of membrane microstructural domains. To gain a deeper understanding of the role of SPFH family proteins at the molecular level, the cryo-EM structures of detergent-purified HflK and HflC complexes derived from *E. coli* were resolved (Ma *et al*. 2022). The structure consisted of SPFH proteins (HflK and HflC) and FtsH, a membrane-anchored AAA+ protease. The HflK/C complex resembled an inverted cup on the membrane, with the walls formed by 12 copies of the HflK-HflC dimer arranged in a circle. Four FtsH hexamers were exclusively located within the cup and specifically interacted with the inner surface of the HflK/C wall to form intact HflK-HflC-FtsH (KCF) complexes (Fig. 4A). The resulting structure led to the hypothesis that the HflK/HflC complex functions as a membrane microdomain, as the HflK/HflC complex interacts with the membrane to create a new microdomain that isolates biochemical processes within the cage from the surrounding membrane. The purification of the HflK/C complex using detergent, while informative, did not fully capture its authentic interaction with the cell membrane.

To gain a comprehensive understanding of native membrane-protein interactions, vesicles derived from the HEK293 GnTI$^-$ cell plasma membranes, organelle membranes, and exosome membranes were analyzed using cryo-EM (Fu and MacKinnon, 2024). Flotillin, a member of the SPFH family, was observed as a large truncated cone attached to the membrane surface in all three samples. Flotillin has wide and narrow ends of truncated cones that were attached to the membrane surface. There was variation in the orientation of Flotillin cages on vesicles, with 40% of Flotillin cages located inside the vesicle (outside-out vesicles), 20% located outside the vesicle (inside-out vesicles) and 40% located outside the vesicle, interacting with other membranes (inside-out double-membrane vesicles) (Fig. 4B).

Notably, the Flotillin cage, situated outside the vesicle, featured a narrow end that could attach to a second membrane by forming hydrophobic surfaces (Fig. 4C). Meanwhile, the attachment of the narrow end of the Flotillin cage to membranes could alter the local curvature of the membrane, thereby influencing endocytosis and mechanosensory processes (Frick *et al*. 2007; Rienzo *et al*. 2009). This provided a new perspective for understanding the native interactions between membrane proteins and membranes. In addition, outward-facing and inward-facing Flotillin cages, displayed notable conformational differences at the membrane interface. However, it was recognized that these vesicles do not accurately replicate the orientation of Flotillin cages within the cell. Investigations utilizing cryo-ET to examine unroofed erythrocytes demonstrated that Flotillin cages embedded within the erythrocyte membrane were arranged in an outside-out

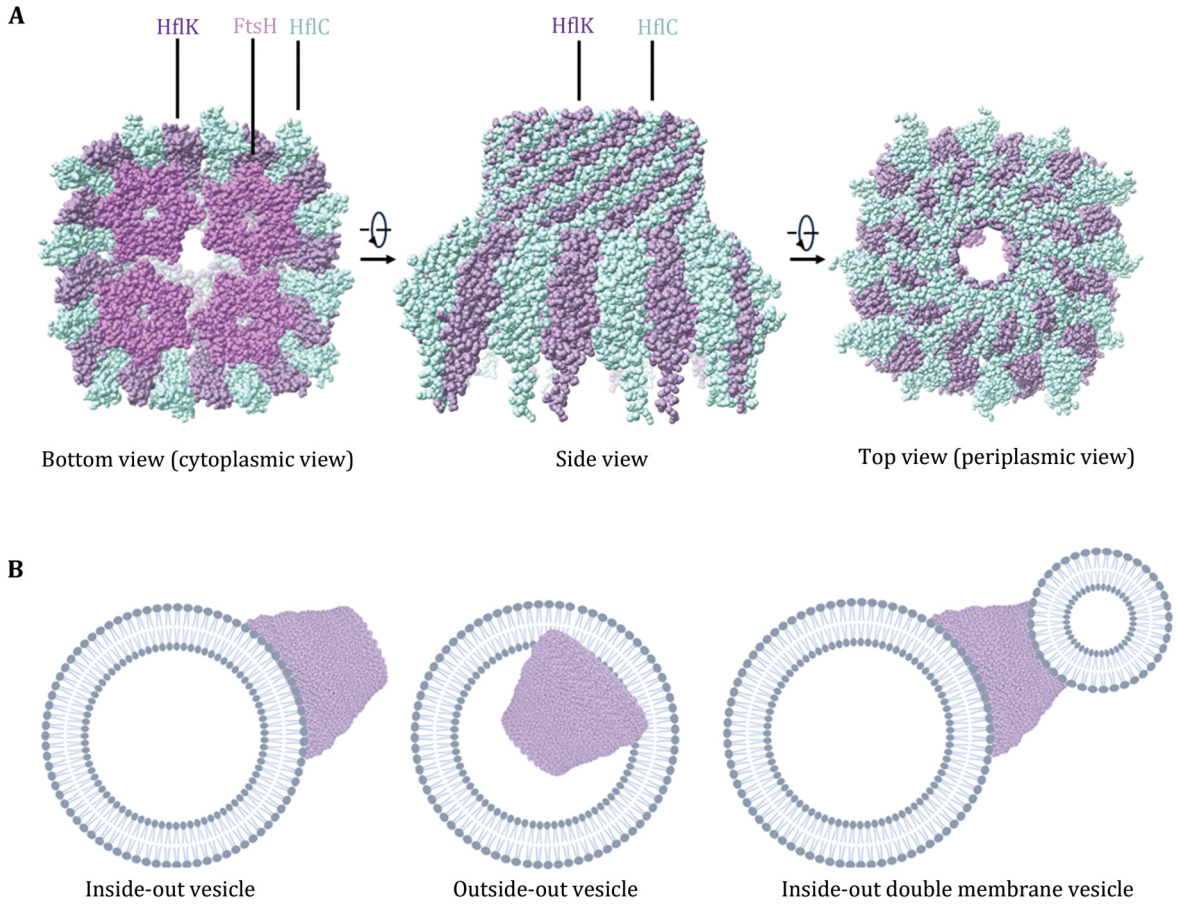

Fig. 4 Structure of the SPFH Family Complex. **A** The overall structure of the intact HflK-HflC-FtsH (KCF) complex. The bottom view (cytoplasmic view), side view and top view (periplasmic view) of the KCF complex (PDB ID 7VHP) are shown in the sphere style. Subunits of HflK, HflC and FtsH are colored lavender, sky blue and dark magenta, respectively. **B** Reconstruction of the Flotillin complex (PDB ID 9BQ2, the biological assembly is shown in the sphere style) associated with the vesicle. 20% of Flotillin is present in inside-out vesicles (left), 40% is located inside outside-out vesicles (middle), and 40% is found in inside-out double-membrane vesicles (right). The Flotillin complex is shown in violet. The membrane is depicted in gray

orientation (Fu and MacKinnon, 2024). This phenomenon suggests that the appearance of inside-out vesicles in the reconstitution of Flotillin liposome may result from their flipping from the original outside-out state. It is also possible that Flotillin, in an inside-out state, may be located on the organelle membrane, where it interacts with the plasma membrane to collaboratively maintain the stability and functionality of membrane microdomains, alongside the outside-out state of Flotillin on the plasma membrane. However, these hypotheses, have not yet been verified as Flotillin cages in an inside-out conformation have not been observed in erythrocyte membrane samples.

Dynamin channels

Dynamin is a membrane-remodeling protein that assembles helical polymers on membranes (Ferguson and De Camilli 2012). Additionally, it exhibited GTPase activity, which was essential for membrane scission during endocytosis (Sundborger *et al*. 2014). In order to elucidate the structure of the dynamin protein, researchers employed lipids to stabilize the interaction between dynamin and membranes *in vitro*, thereby inducing the lipid vesicles to assume a tubular configuration (Dar *et al*. 2015; Jimah *et al*. 2024; Kong *et al*. 2018; Sundborger *et al*. 2014; Sweitzer and Hinshaw 1998; Takei *et al*. 1995). This method helped to preserve dynamin's natural conformation and membrane interactions, therefore providing a more accurate representation of its function within the cell.

In a recent study, dynamin was successfully reconstituted into lipid tubules *in vitro* and observed by cryo-ET (Jimah *et al*. 2024). Dynamin formed a constricted structure in the bound state with GTP, whereas in the GDP-bound state, dynamin was capable of forming a

super-constricted structure, which may represent the final step in membrane fragmentation. In this super-constricted state, novel interfaces between neighboring GTPase molecules were observed (Fig. 5A), which was not evident in the GTP-bound constricted state. In the GDP-bound constricted state, the conformation of the contiguous bundle-signaling element (BSE) was similar to that observed in the GTP-bound state, which is in the "up" position (Fig. 5B). In contrast, the previously solved crystal structure showed BSE remains in the "down" position after GTP hydrolysis (Anand 2016). This may reflect the transition state of kinesin after GTP hydrolysis, preparing for membrane cleavage (Fig. 5C).

In the super-constricted state, the density of the variable loops 1 and 4 of Dynamin's PH (pleckstrin homology) domain, which is known to bind lipids was markedly enhanced in comparison to the crystal structure (Faelber *et al*. 2011) (Fig. 5D). The PH domain rich in positively-charged residues was thus stabilized, and able to form an electrostatic interaction with the membrane surface. The flexibility and dynamics of the PH domains also allowed them to adapt to different membrane curvatures and lipid compositions, thus permitting dynamin to function in different types of membrane environments. In contrast, in the absence of lipid membranes, the PH structural domain was entirely unresolved in the 2-initial GMPPCP-binding structure of the dynamin helix (Liu *et al*. 2021).

GTP hydrolysis played a pivotal role in the interaction of dynamin with lipid tubules and the subsequent membrane super-constricted structure. Dynamin assemblies observed in HeLa cells by cryo-ET exhibited a wide range of diameters (Jimah *et al*. 2024). This finding further corroborated the hypothesis that dynamin was capable of adapting to different sizes of lipid tubules, thereby facilitating membrane contraction and division. The use of cryo-ET was crucial for this research, as it offered a unique opportunity to directly observe dynamin assemblies within the cellular environment. This allows researchers to gain deeper insights into how dynamin orchestrates structural changes, which were essential for membrane contraction and division as well as downstream biological processes including intracellular substance transport and signaling.

Torpedo cholinergic membranes

Nicotinic acetylcholine receptor (nAChR) has been studied both in detergent and *in situ* in the surrounding phospholipid and cholesterol arrangements in Torpedo cholinergic membranes (Unwin 2022).

Upon extraction of the nAChR from the membrane and dissolution in detergent, the transmembrane α-helices exhibit displacement towards the interior of the membrane likely due to the loss of natural membrane constraints (Rahman *et al*. 2020; Unwin 2020). This resulted in a tighter packing of the helices compared to their arrangement in the native state within the membrane.

There were notable discrepancies between the detergent-solubilized and *in situ* structures. In the natural environment of the membrane, the transmembrane α-helices of nAChR were more sparsely arranged. A distinctive transmembrane α-helix situated within the α-subunit of nAChR was found to be more parallel to the membrane surface, as expected to reflect their natural arrangement in the membrane. The peripheral helices of the α-subunit exhibit specific bending and bifurcation features in the region of the outer head groups, which differ from those observed in the detergent. The receptor base may be linked to proteins such as rapsyn, displaying unassigned densities (Zuber and Unwin 2013). These features were absent or less pronounced in the detergent-solubilized structure.

The *in situ* structure also demonstrated the existence of nAChR interactions with lipids. The specific arrangements of cholesterol and phospholipids can form different membrane phases, such as lipid rafts, which are regions of low membrane fluidity that may act as signaling platforms and influence receptor aggregation and activity (Lingwood and Simons 2010; Unwin 2024). The cholesterol molecules within the cell membrane exhibit an alignment that is oriented along the rows (Fig. 6), with a slight variation in tilt angles, closely resembling the linear arrays of cholesterol in a triclinic crystal layer.

Mammalian respiratory supercomplexes

By employing cryo-ET to capture mammalian respiratory supercomplexes (SCs) in their native configuration extracted from porcine heart mitochondria, two novel supercomplex forms, designated as type B ($I_1III_2IV_2$) and type X ($I_2III_4IV_2$) were identified (Fig. 7), suggesting that respiratory chain complexes may have higher-order, more diverse assembly forms under *in vivo* conditions (Zheng *et al*. 2024).

Furthermore, the researchers obtained high-resolution structures of multiple reaction intermediates in the respiratory chain supercomplex, including complex I(CI), which exhibited different states of binding to UQ (Ubiquinone) and UQH2 (Ubiquinol). These structures reflected the dynamics of the respiratory chain supercomplex. Based on the known mechanism of exchange of ubiquinone and ubiquinol, the *in situ*

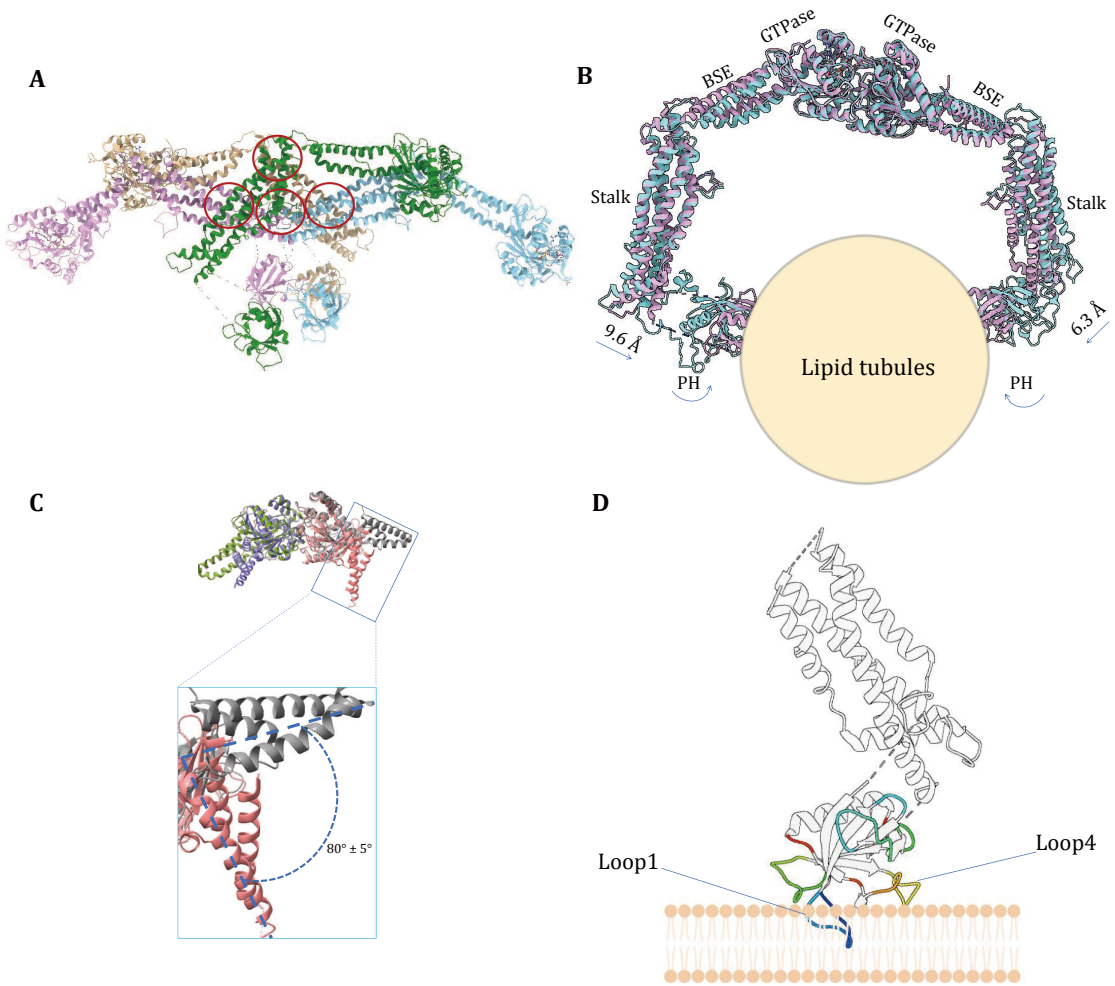

Fig. 5 Comparison of the BSE structural domains of dynamin in the GDP-bound state. **A** New interaction interfaces between neighboring GTPase molecules observed in the super-constricted state (indicated by the red circles). **B** Overlay of the GDP bound super-constricted (pink, PDB ID 8T0R) and GMPPCP (GTP analogs) bound constricted dimers (blue, PDB ID 6DLU), around the GTPase dimer interface. The stalk moves toward the membrane upon GTP hydrolysis 6.3 Å for the kinked, stable monomer (indicated by an asterisk), and 9.6 Å for the flexible monomer. **C** In the lipid tubule structure of GDP-bound dynamin (PDB ID 8SZ8), BSE is in an upward position in the super-constricted state (shown in gray and green respectively for the two monomers). In the crystal structure of GDP-bound dynamin, however, BSE is in a downward position (PDB ID 5D3Q) (shown in red and violet respectively for the two monomers). **D** Dynamic protein helix assembly structure bound to the lipid membrane, exhibiting variable loops in color, among which Loop 1 and Loop 4 interact with the membrane (PDB ID 8SZ4). Adapted from reference (Jimah *et al*. 2024)

structure of CIII revealed the Q cycling process of key intermediates, including the oxidation of QH2 (Ubiquinol) and the reduction of Q (Coenzyme).

The crystal structure of CIII bound to the known Qo site (An active site in complex III) inhibitor stigmatellin was more closely aligned with the head group of the inhibitor stigmatellin bound to CIII than with the endogenous QH2 captured in the *in situ* structure (Huang *et al*. 2005). This proximity may influence the electron acceptance of the ISP (Rieske iron-sulphur protein), potentially leading to the inhibition of CIII activity. Furthermore, four distinct Q-binding states were resolved, suggesting that electron transfer was from QH2 to Cyt c1, mediated by the Rieske structural domain (Crofts *et al*. 1999; Zhang *et al*. 1998).

The presence of lipid molecules was essential for regulating the activity of the electron transport chain, as well as the mobility of the respiratory chain complex in the membrane and its interactions with other complexes. The two A-type ($I_1III_2IV_1$) supercomplexes were arranged in a head-to-head configuration to form the larger X-type ($I_2III_4IV_2$) complex. This dimerization was

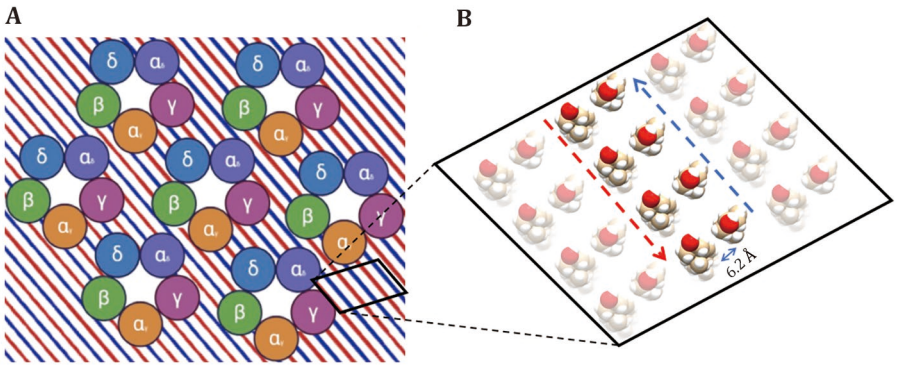

Fig. 6 The arrangement of cholinergic receptors on the membranes of cholinergic cells. **A** Cholinergic receptors are evenly distributed across the cell membrane, with different colored circles indicating different subunits of cholinergic receptors. The red and blue lines represent the staggered and aligned positioning of cholesterol molecules respectively. The size of the cholinergic receptors and cholesterol are not to scale. **B** The arrangement of cholesterol molecules within a triclinic crystal layer. Equivalent rows are identified by red and blue dashed arrows to distinguish and compare the arrangement of cholesterol molecules across different rows, with red representing oxygen atoms, white representing hydrogen atoms, and yellow representing carbon atoms in cholesterol. Adapted from reference (Unwin 2022)

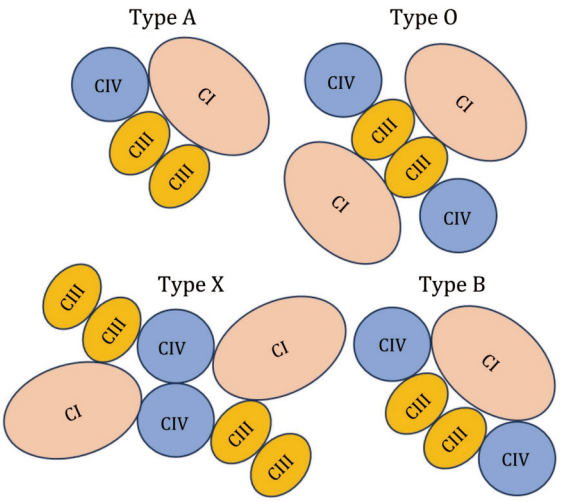

Fig. 7 Different compositions of the respiratory chain supercomplex in mammalian mitochondria. Type A ($I_1III_2IV_1$) represents the most prevalent form of the respiratory chain supercomplex, comprising one complex I (CI), two complexes III (CIII), and one complex IV (CIV). Type O ($I_2III_2IV_2$) supercomplex form contains two complexes I (CI), two complexes III (CIII), and two complexes IV (CIV). Type X ($I_2III_4IV_2$), contains two complexes I (CI), four complexes III (CIII), and two complexes IV (CIV), known as type X because of its chromosome-like appearance. Type B ($I_1III_2IV_2$), comprises one complex I (CI), two complexes III (CIII), and two complexes IV (CIV)

primarily mediated by "protein–lipid–protein" interactions. At the dimerization interface, no other typical strong protein–protein interactions were observed, except for a potentially weak interaction between CI and CIV.

The role of lipid molecules in the supercomplex was to act as a linker and stabilizer between the subunits, filling the interfacial space between the protein subunits and helping to maintain the structural stability of the supercomplex. The assembly of the supercomplex exerted a significant influence on the local curvature of the membrane surrounding it. Furthermore, the geometry of the membrane may also affect the arrangement, distribution, and conformation of the supercomplex. For instance, in the membrane region surrounding CI, the membrane was curved towards the mitochondrial matrix. This curvature contributed to the interactions of CI with other complexes. In contrast to the curvature of the membrane surrounding CI, the membrane in the $CIII_2$ region displayed a curvature towards the mitochondrial intermembrane space. This opposite curvature may influence the lateral migration and sorting of lipids, peptides and proteins, and consequently affect the behavior of small molecules within the membrane (Iversen *et al.* 2015; McMahon and Boucrot 2015). In CI, lipid molecules played a role in facilitating efficient proton transfer pathways.

As a result of the detailed examination of the structure and function of membrane proteins, researchers are coming to recognize that preserving the *in situ* structure of membrane proteins within their natural membrane environment is essential for comprehending their biological functions. As a carrier that mimics the cellular membrane environment, liposomes permit researchers to study the structure and function of membrane proteins under near-physiological conditions. In contrast, the cryo-ET technique enables researchers to directly observe and resolve the 3D structures of proteins in the natural environment of

cells. Nevertheless, cryo-ET technology still presents numerous challenges.

METHODS FOR MEMBRANE PROTEIN STUDIES USING CRYO-EM

In cryo-EM methodologies employed for the study of membrane proteins, sample preparation can be broadly categorized into two overarching strategies, purified samples and *in situ* samples. These two approaches possess distinct advantages and limitations, rendering them suitable for diverse research objectives and experimental conditions. The purified samples approach is suitable for studies aiming for high resolution, while the *in situ* approach is more powerful for studies of membrane protein–lipid interactions and the native structure of membrane proteins.

Sample preparation

Purified samples, including those in detergent micelles, nanodiscs, SMALPs and liposomes, generally exhibit a reduction in impurities, greater homogeneity, and therefore enhanced resolution in cryo-EM structure determination. However, the purification process likely alters the natural environment of the proteins, affecting their structures and functions. In particular, the purification process may result in the loss of lipids that interact with membrane proteins and are vital for their functionality. Thus here we mostly focus on the preparation of *in situ* samples, while details of common sample preparation methods for purified samples can be found in recent reviews (Arnold *et al*. 2018; Weissenberger *et al*. 2021; Xu and Dang 2022).

Given the complex background, for *in situ* samples, gold nanoparticles are frequently used to locate target molecules in cell sections. Techniques such as SNAP-tag-labeled nanogold (Song *et al*. 2015) or immunogold labeling allow specific binding to macromolecules on the outer membrane (Spehner *et al*. 2020). These gold particles appear as high-electron-density black dots under the electron microscope, enabling precise localization of target molecules based on their positions (Griffiths and Lucocq 2014).

Freezing

In the process of *in situ* sample preparation, the sample is rapidly frozen to prevent the formation of ice crystals and thereby maintain the native state of the sample. Rapid freezing methods typically include plunge freezing and high-pressure freezing (HPF).

Similar to purified samples, thin *in situ* samples such as mammalian cells cultured on a cryo-EM grid (Mahamid *et al*. 2016) could be directly immersed in a cryogenic liquid (ethane or propane, *etc*.) to rapidly achieve freezing (Adrian *et al*. 1984; Frederik and Hubert 2005; Iancu *et al*. 2006), known as plunge freezing.

The preparation of larger cell or tissue samples can be achieved through the use of HPF, which employs high pressure (typically 210 MPa) to reduce the freezing point of water, facilitating rapid freezing while minimizing volume expansion during ice formation (Moor *et al*. 1980).

Thinning

To permit effective penetration of the electron beam and acquisition of a clear image, a sample for cryo-EM needs to be sufficiently thin. Therefore, *in situ* samples often require a thinning process, the accuracy and efficiency of which are under active improvement.

CEMOVIS

The CEMOVIS (Cryo-Electron Microscopy of Vitreous Sections) is employed for the preliminary trimming of voluminous samples. Frozen hydrated samples are excised with a diamond knife into continuous slices of an appropriate thickness, and the samples are mounted on special grids for observation in a transmission electron microscope (Al-Amoudi *et al*. 2004). The slices are prepared in the frozen state. This approach better preserves the sample's native state; however, the slices may undergo compression along the direction of the cut, which can interfere with imaging and reconstruction. CEMOVIS enables internal high-resolution 3D imaging of samples that are too thick to be directly imaged in cells or even tissues (Bleck *et al*. 2010).

Cryo-FIB

Cryo-FIB technology employs a combination of cryo-ET and focused ion beam (FIB) techniques at low temperatures for the precise cutting and milling of biological samples in the vitrified state. This is done in order to prepare lamellae suitable for TEM observation (Marko *et al*. 2007; Rigort and Plitzko 2015). The focused ion beams typically use gallium, along with xenon, argon, and others (Schaffer *et al*. 2019). The material is progressively removed from the two sides of the sample material by the ion beam until the desired slice thickness (as low as 10 nm) is reached (Vidavsky *et al*. 2016). The ion beam damage to the sample is reduced

by optimizing the ion beam parameters (*e.g*. beam intensity, beam diameter, and milling time) prior to performing cryo-FIB. The thickness of the sample must be accurately controlled, as this affects the imaging quality and the accuracy of the 3D reconstruction. Subsequently, the sample is dried in a high vacuum environment During the cryo-FIB process, a scanning electron microscopy (SEM) mode is used to monitor the milling process and quality of the samples, ensuring the uniformity and integrity of the slices. Once the preparation of the samples is complete, they are either transferred to a TEM grid or imaged directly by TEM within a FIB-SEM instrument. The application of cryo-FIB technology allows for the precise and controlled preparation of ultra-large samples for cryo-ET. However, it should be noted that ion beam processing may cause some damage to the sample surface, and the sample may be affected by charge accumulation during processing. The recent development of a fully automated sequential cryo-FIB preparation process for high-quality lamellae, which includes rough milling and polishing, has the potential to significantly reduce the time required for thin-section preparation while simultaneously minimizing the user input requirements. This, in turn, has the capacity to enhance the imaging accuracy and applicability to different proteins (Zachs *et al*. 2020).

Cryo-FLM-FIB-ET (cryo-fluorescence light microscopy-focused ion beam-electron tomography)

The novel cryo-FLM-FIB-ET methodology integrates the advantages of cryo-fluorescence light microscopy (cryo-FLM), cryo-FIB milling, and electron tomography (cryo-ET) to achieve high-resolution imaging of biological samples (Yang *et al*. 2023). Initially, biological samples are cryo-fixed to preserve their native structure and imaged using fluorescence microscopy to identify and localize the target area under frozen conditions. Target proteins are labeled with fluorescent probes and visualized through cryo-FLM, enabling precise localization of the target structure (Liedtke *et al*. 2022; Wolff *et al*. 2020; Li *et al*. 2023a, b). Based on the fluorescence imaging results, ultra-thin lamellae are prepared with high precision using cryo-FIB milling, followed by electron tomography under a TEM for nanoscale imaging. This integrated approach allows continuous imaging from the molecular to the nanoscale level while ensuring accurate localization of target structures.

Cryo-FIB lift-out

The cryo-lift-out process enables the precise extraction of targeted regions from vitrified samples in cryo-FIB techniques. After high-pressure freezing, the sample is trimmed using a cryosectioner, and specific areas of interest are identified and prepared through cryo-FLM milling (Hsieh *et al*. 2014; Mahamid *et al*. 2015). In the cryo-lift-out step, these regions are carefully extracted and transferred to a cryo-TEM grid for further thinning and imaging. This method is particularly valuable for isolating specific areas from large, complex frozen samples, such as tissues or whole organisms, that are difficult to access with conventional cryo-FIB milling. By minimizing contamination and damage during sample preparation, cryo-lift-out improves imaging quality and facilitates reliable analysis of intricate biological structures, including organelles, membranes, and cell–cell interactions (Kuba *et al*. 2021).

Plasma cryo-FIB

Plasma cryo-FIB represents a novel approach to sample preparation for structural biology, whereby a plasma ion source is employed in lieu of a traditional metal ion source, such as gallium. The plasma source produces ions with greater energy, which interact with the sample in a more efficient manner, thereby reducing the physical damage to the sample. The higher ion energy produced by the plasma enables the use of a lower ion dose when cutting the sample, thereby increasing the efficiency of sample preparation, reducing damage to the sample surface, and enabling the fine grinding required for thinner, more fragile samples (Bassim *et al*. 2014).

Waffle

The Waffle method is a cryo-FIB technique that involves the use of a waffle-shaped specimen holder. The Waffle method is suitable for processing tissue sections or cell suspensions up to tens of microns in thickness. It is also applicable to thicker samples that are not suitable for conventional cryo-FIB methods, such as tissue sections or cell clusters. The samples are rapidly frozen by high-pressure freezing and subsequently sectioned using a cryo-FIB, resulting in thin slices that are suitable for cryo-ET analysis. The samples are then cut into a waffle-like lattice structure, which is referred to as the "Waffle" structure. The grid-like structure facilitates the localization and identification of specific sample regions in subsequent cryo-ET analysis. The cut samples are then transferred to a TEM grid for further imaging and analysis. This method is particularly suitable for studying 3D structures at the tissue level, yet the thickness and complexity of the sample may also impact the imaging quality and resolution of cryo-ET (Kelley *et al*. 2022; Klykov *et al*. 2022).

Data collection

The data collection process for single-particle cryo-EM has been well established (Cheng and Yu 2024; Koh *et al*. 2022; Weis and Hagen 2020). For cryo-ET, a series of projected images is recorded during data collection in order to obtain a tomographic image of the region of interest while tilting the sample. Following the refinement of the center height at the recording position, each image in the series must be tilted, centered, focused, and recorded (Turk and Baumeister 2020). The images of the sample at different tilt angles are collected to form a tilt series, which enables 3D reconstruction.

Tilt scheme

The dose-symmetric tilt scheme begins with a zero-degree tilt and gradually increases the tilt angle symmetrically in both positive and negative directions (Hagen *et al*. 2017). For instance, with a 3° tilt step, images are collected in the sequence: 0°, +3°, −3°, +6°, −6°, and so on. By capturing low tilt angle images early in the tilt series, when the sample appears thinner, it is possible to acquire more high-resolution information before radiation damage accumulates. This scheme, when combined with a phase plate, enhances the contrast of TEM images by modifying the phase rather than the amplitude of the electron wave under low-dose conditions (Winter and Chlanda 2021). Compared to bidirectional tilt schemes, the dose-symmetric tilt scheme avoids alignment difficulties caused by "jump-at-start" issues (Fig. 8), where cumulative dose differences between branches make alignment challenging (Parkhurst *et al*. 2024). It ensures smoother cumulative electron dose distribution throughout the tilt series, reducing deformation and allowing for higher total electron doses at larger tilt angles. Additionally, the larger tilt range enables the discarding of high-tilt or late-stage images without compromising the quality of the collected data.

Hardware

For cryo-ET, hardware innovations, including direct electron detectors, energy filters, and phase plates, have become critical to improving both imaging quality and resolution. Direct electron detectors represent a major leap forward by converting incident electrons directly into digital signals without relying on indirect detection (Mendez *et al*. 2019). This technology significantly enhances sensitivity, allowing for imaging at lower electron doses and reducing radiation damage to delicate samples (McMullan *et al*. 2016). Recent advancements, particularly with the Apollo detector, have pushed these capabilities even further. The Apollo's exceptional dynamic range and faster readout speeds enable the simultaneous achievement of both high throughput and high resolution, two goals that were previously difficult to balance. This breakthrough allows for the rapid capture of more data, thus enhancing the efficiency of cryo-ET workflows without compromising resolution (Peng 2023). Combined with advanced automation and preparation techniques, direct electron detectors have become indispensable in achieving subnanometer resolution (Sheng *et al*. 2022).

Energy filters further enhance imaging quality by permitting only electrons that haven't lost energy to pass through, improving both contrast and resolution. The Zero-Loss Filtering (ZLF) technique eliminates inelastically scattered electrons, thereby reducing chromatic aberration, background noise, and radiation damage. It helps preserve the native state of biological samples even under low-dose conditions, allowing for more accurate structural analysis. In parallel, phase plates improve contrast by modulating the phase of transmitted electrons (Ruiz Caridad *et al*. 2022). The Volta phase plate (Fan *et al*. 2017), for example, introduces a controlled phase delay to enhance contrast while minimizing radiation damage, a crucial advancement for imaging sensitive biological structures. When paired with energy filters, phase plates enable detailed elemental and chemical state analysis, pushing the limits of what cryo-ET can reveal. More recently, the Ponderomotive Phase Plate (Du and Fitzpatrick 2023), inspired by the Zernike phase plate from light microscopy, uses laser field potential energy to manipulate electron phases, further improving contrast and resolution in biological samples.

Software

While cryo-ET data collection used to be quite time-consuming compared to SPA, automated software processes have made it faster and easier. Software like PACEtomo allows for the simultaneous collection of projections from multiple positions, significantly reducing data acquisition time and increasing throughput (Eisenstein *et al*. 2023). Tomo Live enables real-time tilt-series alignment, reconstruction, and quality assessment, offering immediate feedback and making it easier to optimize data collection as it occurs (Comet *et al*. 2024). SerialEM has advanced to provide full automation of tilt-series acquisition, allowing users to set parameters for entire data collection sessions, thus minimizing user intervention (Schorb 2019). Legion

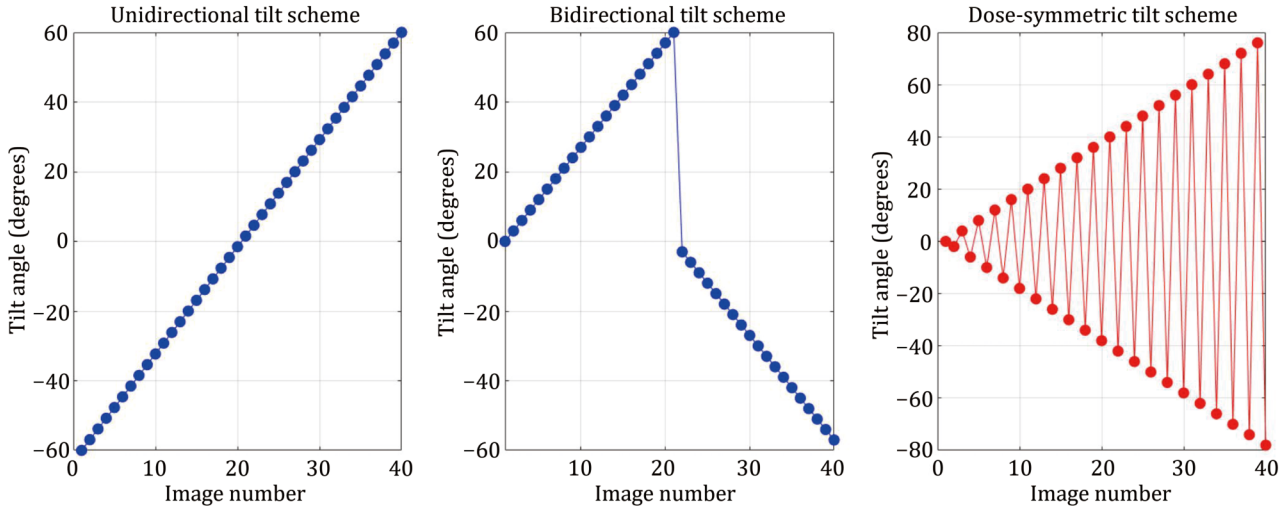

Fig. 8 Tilt scheme for cryo-ET. The tilt angles for the unidirectional tilt scheme, bidirectional tilt schemes, and dose-symmetric tilt schemes as a function of the image number. Each circle represents one image collected at the indicated tilt angle

has been updated to provide compatibility with a broad range of standard TEMs, making automated cryo-ET data collection more accessible without requiring specialized equipment (Karimi *et al*. 2024).

Data processing

Recent advances in the data processing techniques of both single-particle analysis (SPA) and tomography are described to assist structural biologists in studying membrane proteins.

SPA

As long as the membrane protein of interest is stabilized in detergent, nanodiscs, or SMALPs, SPA processing is generally similar to that of soluble protein. Steps that are particularly critical for membrane proteins, especially for proteoliposome samples, are discussed here.

Particle picking

To eliminate the interference caused by lipid signals, the "signal subtraction" method was employed to facilitate visualization of proteins embedded in liposome membranes (Tonggu and Wang 2018). However, this method has several limitations: (1) the need for individual reprocessing of all original micrographs; (2) the requirement of liposomes to be perfect spheres; and (3) the high precision required for each liposome's size fitting and signal scaling to avoid artifacts during signal subtraction. Therefore, picking membrane protein particles with their surrounding lipids has become more mainstream. To complete this challenging task, a series of neural network-based particle-picking pipelines have been trained, including EMAN2 (Bell *et al*. 2018), APPLE picker (Heimowitz *et al*. 2018), *WARP* (Tegunov and Cramer 2019), SPHIRE-crYOLO (Wagner *et al*. 2020), Topaz (Bepler *et al*. 2019), CASSPER (George *et al*. 2021), among others.

Topaz could be utilized for the structural analysis of liposomal membrane proteins, yet not particularly effective at distinguishing between proteins that were embedded in intact vesicle membranes and those in damaged vesicles or lipid bilayer plaques (Fu and MacKinnon 2024). Vesicle Picker, on the other hand, could autonomously identify vesicles in cryo-EM maps and unsupervisedly select particles associated with those vesicles (Karimi *et al*. 2024). Using the highest quality particle images provided by the Vesicle Picker to seed Topaz models could maximize the number of particle images available for 3D reconstruction.

Post processing

Reconstructed 3D density maps often need to be post-processed to compensate for the loss of contrast and details to reveal structural information of a higher resolution. The post-processing approaches could be categorized into map sharpening (Rosenthal and Henderson 2003), density modification (Terwilliger *et al*. 2020a, b), and refinement (Urzhumtsev *et al*. 2022).

The expected outcome of map sharpening was to

enhance the representation of anticipated molecular features at a specified resolution by improving the contrast of the map. The global map sharpening affected all regions uniformly, whereas the signal-to-noise ratios of maps typically differed from one region to another (Rosenthal and Henderson 2003; Terwilliger *et al*. 2018). Consequently, global filtering may lead to excessive blurring in high-resolution areas or oversharpening in low-resolution areas of the map. To address the aforementioned issues, techniques for local sharpening have been developed. LocalScale could locally sharpen a map based on an existing atomic reference structure (Jakobi *et al*. 2017). LocalDeblur was particularly suitable for membrane proteins with a high degree of flexibility (Ramírez-Aportela *et al*. 2020). LocSpiral enabled molecular modeling on maps with flexibility and slightly anisotropic resolution (Kaur *et al*. 2021). DeepEMhancer was based on a convolutional neural network that facilitates the post-processing of experimental maps, executing both masking and sharpening operations in a single step (Sanchez-Garcia *et al*. 2021).

The fundamental principle of density modification is to adjust experimentally obtained maps using limited experimental data, in conjunction with established principles such as structure factor amplitudes and phase sets (Terwilliger 2000). These methods were suitable for maps that had preliminary knowledge or established structures of similar macromolecules (Terwilliger *et al*. 2020a, b).

Post-processing can also be achieved through refinement to further optimize the atomic model. Servalcat could visualize weak features, including hydrogen density (Yamashita *et al*. 2021). M40 used a powerful contrast transfer function (CTF) correction method and neural network-based map noise reduction to achieve higher resolution across multiple datasets (Tegunov *et al*. 2021).

Model building

Although electron density maps with a resolution of 2–4 Å cannot distinguish individual atoms, reliable atomic models can be constructed using prior knowledge of the chemical structures of proteins and nucleic acids in the samples, including their amino acid and nucleic acid sequences. Previously, building atomic models required researchers to manually operate programs such as *COOT* (Emsley *et al*. 2010) and ISOLDE (Croll 2018). With the advancement of artificial intelligence and machine learning, deep learning techniques for automated atomic model construction are being proposed (see Table 1). These methods could help the identification of density maps without known sequences of proteins and facilitate the building of atomic models from these maps.

In particular, the predictive modeling tools AlphaFold (Jumper *et al*. 2021) and RoseTTAFold (Baek *et al*. 2021) could predict the 3D structures of a wide range of individual proteins and small complexes based on their amino acid sequences. By combining SPA with predictive modeling tools, researchers could resolve macromolecular structures in difficult cases (Corum *et al*. 2024; Sun *et al*. 2023; Tai *et al*. 2022).

Tomography

Cryo-ET is particularly well-suited for investigating membrane proteins *in situ* in the context of macromolecular complexes and organelles, even dynamic processes such as vesicle transport and membrane fusion. Careful processing of the tilt series data is critical to uncover useful information in a crowded and noisy environment.

Tilt series alignment

Tilt series alignment (TSA) is a crucial step for obtaining high-resolution 3D reconstructions. With the development of high-throughput tomography data collection techniques, there is an increasing need for highly accurate and fully automated tilt series alignment. Dynamo (Castaño-Díez 2017) and IMOD (Kremer *et al*. 1996; Mastronarde and Held 2017) are popular software packages widely used for tilt series alignment. In addition, TomoAlign integrated tools that could simultaneously handle beam-induced sample motion and the microscope's CTF, which were particularly well-suited for aligning thick samples (Fernandez and Li 2021). AreTomo aligned and reconstructed markerless chromatography images using fully automated motion correction (Zheng *et al*. 2022). More recently, Markerauto2 facilitated the alignment of imaging based on the alignment of reference markers, and the software was fully automated to enhance usability for researchers (Xu *et al*. 2024b).

3D reconstruction and reduction of Missing Wedge

In tomography data processing, the missing wedge problem impacts the reconstruction of a complete 3D volume. During tilt series collection, the inability to rotate the sample by ±90° leads to a loss of information in Fourier space, known as a missing wedge, which causes elongation artifacts in the reconstructed tomographic image. The most common data acquisition

Table 1 Deep learning methods for automatic atomic model building

Methods	Year	Function	Open source
Structure Generator (Li *et al*. 2020)	2020	A fully automated, template-free model-building method based entirely on neural networks.	√
Cascaded CNN (Si *et al*. 2020)	2020	CascadedCNN predicted secondary structure elements (SSEs), main chain structures, and Cα atoms, generating comprehensive prediction maps.	√
Haruspex (Mostosi *et al*. 2020)	2020	Haruspex could be directly applied to newly reconstructed maps to support domain layouts or serve as a starting point for main chain layouts.	√
DeepTracer (Pfab *et al*. 2021)	2021	DeepTracer was utilized to quickly ascertain the structure of multi-chain protein complexes based on high-resolution cryo-EM images from the ground up.	×
EMNUSS (He and Huang 2021)	2021	EMNUSS featured an innovative secondary structure annotation framework designed for medium- to high-resolution cryo-EM maps.	√
DeepTracer ID (Chang *et al*. 2022)	2022	DeepTracer could help users identify candidate proteins in provided organisms without additional information by generating a model of the protein backbone that best represented the cryo-EM profile and subsequently searching for that model in the AlphaFold2 prediction library.	×
CR-I-TASSER (Zhang *et al*. 2022)	2022	CR-I-TASSER predicted Cα positions using deep learning, significantly enhancing the quality of threading templates and, consequently, the accuracy of the final model through optimized fragment assembly simulations.	√
EMBuild (He *et al*. 2022)	2022	EMBuild integrated AlphaFold structure prediction, FFT-based global fitting, domain-based semi-flexible refinement, and iterative graph-based assembly, all built upon a probabilistic map of the main chain predicted by a deep convolutional network. This advanced approach enabled the automatic construction of multi-chain protein complexes from medium-resolution cryo-EM maps.	√
ModelAngelo (Jamali *et al*. 2024)	2024	ModelAngelo constructs protein atom models and nucleotide backbones with high precision, aiding in the identification of proteins with unknown sequences.	√
DeepTracer-Refine (Chen *et al*. 2024)	2024	DeepTracer-Refine accurately determines protein structures by aligning AlphaFold predictions with the modeled structures of DeepTracer.	√
Cryo2Struct (Giri and Cheng 2024)	2024	Cryo2Struct was a fully automated *ab initio* cryo-EM structure modeling method that utilizes a 3D converter to identify atoms and amino acid types in cryo-EM density maps. It employed innovative Hidden Markov Models (HMMs) to link the predicted atoms and construct the protein backbone structure.	√
CryFold (Su *et al*. 2024)	2024	CryFold had enhanced ModelAngelo by incorporating the latest advancements from AlphaFold2. This integration allowed for high-speed, accurate, and automated construction of models based on cryo-EM maps of multi-protein complexes with unknown compositions.	√

strategy was uniaxial tomography, in which the sample was rotated around a single axis during imaging (Han *et al*. 2017). To minimize missing data regions in tomography, biaxial tomography was employed. This technique reduced the areas of missing data by rotating the image around two mutually perpendicular axes, effectively transforming the "missing wedge" problem into a smaller "missing pyramid". The Etomo (Mastronarde and Held 2017) and AuTom-dual (Winter and Chlanda 2021) tools in the IMOD and PEET software packages could be utilized for the more challenging alignment of the two perpendicular orientations.

As uniaxial imaging of tomography remains the more common strategy, in recent years, neural network methods have been employed to minimize the missing wedge. The Joint Deep Learning Model (JDLMID) filled in the missing wedges through image restoration (Ding *et al*. 2019). IsoNet was a neural network method designed to reconstruct missing wedge information and to enhance the signal-to-noise ratio (SNR) through five steps: CTF deconvolution, mask generation, extraction, refinement and prediction (Liu *et al*. 2022). The refine-

ment step is trained on a pair of tomograms to extract subtomograms that still contain missing wedges. IsoNet then iteratively updated the predicted pair of subtomograms to fill in the missing wedges with predicted information using deep learning techniques. DeepDeWedge was a deep learning-based method designed for denoising and reconstructing missing wedges in tomography, which could produce an overall sharper reconstruction with higher contrast (Wiedemann and Heckel 2024).

In addition, several tools utilized in SPA can be employed together to aid in the 3D reconstruction of tomography. RELION-4.0 also performs CTF refinement and tilt sequence refinement with M serving as an external tool (Zivanov *et al*. 2022). A bi-directional interface can be created between the Dynamo and the Warp-RELIION-M pipeline, which can provide a framework for *ab initio* and geometric approaches to multiparticle refinement in M (Burt *et al*. 2021).

Model building

The resolution achieved by cryo-ET is usually insufficient for atomic model building. By utilizing STA and classification, it is possible to amplify the signals of particles belonging to the same type of macromolecule, thereby obtaining much higher resolution structures (Förster 2022). Once the tomographic density map reaches the sub-atomic resolution, the model-building process is similar to that of SPA.

In recent years, the STA program has rapidly evolved toward full automation. One of the challenges of STA is the masking and filtering of the averaged volume after each refinement iteration. As the intracellular target protein is surrounded by other high-density proteins and lipids, masking in STA can significantly affect the final resolution on the target protein. EMAN2.3 could retain high-resolution information of the target protein for subsequent rounds of refinement and minimize misalignment caused by surrounding densities (Chen *et al*. 2019).

EmClarity is a graphics processing unit (GPU)-accelerated image processing software that provides functions including STA and classification for macromolecular complexes at high resolution (Ni *et al*. 2022). EmClarity could calculate the contrast transfer function (CTF) modulation effect, update 3D sampling functions (3DSF), according to missing wedge information, at every processing step, and employ a multi-scale, 3DSF-weighted classification method to improve the tilt-series alignment. This method was particularly well-suited for low-temperature focused ion beam milling of thin section recordings for tomography datasets.

TomoBEAR was a modular and configurable workflow engine designed to streamline the processing of cryo-ET data for STA (Balyschew *et al*. 2023). It can be applied to high-resolution structural analysis of membrane proteins in plasma FIB-milled lamellae. RELION5 introduces a pipeline for analyzing tomography data, ranging from importing unprocessed movies to automated atomic modeling in high-resolution STA maps (Burt *et al*. 2024). While different software packages utilize varying inputs, outputs, and file formats in the extensive image processing tasks, TOMOMAN (TOMOgram MANager) stores the metadata of the tomographic image processing in a MATLAB structured format and manages the inputs, outputs, and executions of external packages (Khavnekar *et al*. 2024).

CONCLUSION AND PERSPECTIVES

Membrane proteins play crucial roles in various biological processes and are important targets for drug discovery. Various strategies have been developed to extract and stabilize these proteins and their partners for structural and functional investigations, each with its advantages and limitations.

Nanodisc is one popular approach for membrane protein stabilization. It offers the benefits of homogeneity and consistent stability, providing a platform that mimics the biological membrane environment. However, its technical demands, including size limitations (8–20 nm), can restrict protein conformation and lipid dynamics, potentially affecting the functional studies of membrane proteins. SMA copolymers present an alternative strategy that outperforms traditional detergents in terms of maintaining membrane protein stability and applicability in drug screening. Nonetheless, this method requires high concentrations and solubility of membrane proteins, which may lead to phase separation and subsequent solubilization in lipids. Reconstituting membrane proteins into liposomes has also proven effective in maintaining an intact membrane environment, thereby facilitating the study of voltage-gated ion channels, proton-driven transporters, and mechanosensitive ion channel proteins. However, this approach is not suitable for membrane proteins that require stabilization in detergents with low critical micelle concentrations. The *in situ* analysis has emerged as a promising method for elucidating membrane protein structure under physiological conditions. This technique, however, often relies on advanced algorithms and high-performance computational hardware, which may limit its accessibility and application.

Despite the substantial progress that has been made in methods for extracting membrane proteins and analyzing their structures, we believe that better models—born from the integration of artificial intelligence (AI)—will assist in data processing, 3D reconstruction, and model building, thereby achieving higher resolution. AI technology automates data preprocessing, image segmentation, and feature extraction, reducing dependence on specialized personnel and extensive manual intervention. Additionally, AI algorithms swiftly identify critical regions like cells, particles, or nanostructures, significantly minimizing manual operation time costs. Furthermore, through deep learning models, AI discerns intricate microstructural features such as crystallographic defects and nanoparticle arrangement patterns. Since its inception, AlphaFold has captivated the scientific community with its exceptional accuracy in predicting static protein structures (Jumper *et al*. 2021). The recent update, AlphaFold3, further enhances its capabilities by enabling the prediction of protein complex structures, marking significant progress in the field (Abramson *et al*. 2024). Nevertheless, the results derived from AlphaFold predictions cannot fully substitute for experimental structural determinations, as the latter frequently exhibit superior accuracy (He 2025), particularly in domains such as structure-guided drug design (Karelina *et al.* 2023; Scardino *et al.* 2023; Wong *et al.* 2022), where meticulous optimization of chemical compounds is essential. Thus, it is evident that structures determined experimentally using methods such as cryo-EM or X-ray crystallography will remain the gold standard for the foreseeable future.

Nonetheless, it is worth noting that AI has significantly empowered and revolutionized the field of structural biology, which is currently experiencing substantial growth. In recent years, there has been an explosion in the development of dynamic prediction models for protein complexes, particularly those membrane proteins, as these are critical receptors in drug development. For example, a generative AI method called SurfDock has been developed for predicting protein–ligand complex structures (Cao *et al* 2025). This innovative model integrates various protein data into a cohesive representation at surface nodes, potentially offering new insights into predicting not only ligand but also lipid interactions at protein interfaces. Moreover, a geometric deep generative model named DynamicBind has been created for the dynamic structural prediction of complexes, providing notable advantages for studying lipid-membrane protein interactions due to the highly dynamic nature of lipids (Lu *et al*. 2024). Another approach, PeSTo, is a non-parametric geometric deep learning method that accurately predicts interfaces between proteins and various biomolecules, including lipids, nucleic acids, ions, and small molecules (Krapp *et al*. 2023). Furthermore, a novel method known as the AF2-mutation framework has been experimentally validated, demonstrating that specific mutations in SPNS2, a transmembrane lipid transporter, induce significant conformational changes in the protein structure, thus providing compelling evidence of the potential for artificial intelligence to accurately forecast the intricate dynamic alterations of membrane protein conformations (Yuan *et al*. 2024). These methods will likely function as a formidable asset in elucidating the intricate mechanisms underlying the dynamic interactions between membrane proteins and lipids.

Acknowledgements This work was supported by the National Natural Science Foundation of China (32222037 to Yusong R. Guo).

Compliance with Ethical Standards

Conflict of interest Sixian He, Yun Han, Xinying Liu and Yusong R. Guo declare that they have no conflict of interest.

Human and animal rights and informed consent This article does not contain any studies with human or animal subjects performed by the any of the authors.

References

Abramson J, Adler J, Dunger J, Evans R, Green T, Pritzel A, Ronneberger O, Willmore L, Ballard AJ, Bambrick J, Bodenstein SW, Evans DA, Hung C-C, O'Neill M, Reiman D, Tunyasuvunakool K, Wu Z, Žemgulytė A, Arvaniti E, Jumper JM (2024) Accurate structure prediction of biomolecular interactions with AlphaFold 3. Nature 630(8016): 493–500

Adrian M, Dubochet J, Lepault J, McDowall AW (1984) Cryo-electron microscopy of viruses. Nature 308(5954): 32–36

Al-Amoudi A, Chang J-J, Leforestier A, McDowall A, Salamin LM, Norlén LPO, Richter K, Blanc NS, Studer D, Dubochet J (2004) Cryo-electron microscopy of vitreous sections. EMBO J 23(18):

3583–3588
Anand R, Eschenburg S, Reubold TF (2016) Crystal structure of the GTPase domain and the bundle signalling element of dynamin in the GDP state. Biochem Biophys Res Commun 469(1): 76–80
Anderluh A, Hofmaier T, Klotzsch E, Kudlacek O, Stockner T, Sitte HH, Schütz GJ (2017) Direct PIP(2) binding mediates stable oligomer formation of the serotonin transporter. Nat Commun 8: 14089. https://doi.org/10.1038/ncomms14089
Arnold SA, Müller SA, Schmidli C, Syntychaki A, Rima L, Chami M, Stahlberg H, Goldie KN, Braun T (2018) Miniaturizing EM sample preparation: opportunities, challenges, and 'visual proteomics'. Proteomics 18(5–6): e1700176. https://doi.org/10.1002/pmic.201700176
Ayub H, Murray RJ, Kuyler GC, Napier-KhwajaF, Gunner J, Dafforn TR, Klumperman B, Poyner DR, Wheatley M (2024) GPCRs in the round: SMA-like copolymers and SMALPs as a platform for investigating GPCRs. Arch Biochem Biophys 754: 109946. https://doi.org/10.1016/j.abb.2024.109946
Azhar S (2010) Peroxisome proliferator-activated receptors, metabolic syndrome and cardiovascular disease. Future Cardiol 6(5): 657–691
Baek M, DiMaio F, Anishchenko I, Dauparas J, Ovchinnikov S, Lee GR, Wang J, Cong Q, Kinch LN, Schaeffer RD, Millán C, Park H, Adams C, Glassman CR, Degiovanni A, Pereira JH, Rodrigues AV, van Dijk AA, Ebrecht AC, Opperman DJ, Sagmeister T, Buhlheller C, Pavkov-Keller T, Rathinaswamy MK, Dalwadi U, Yip CK, Burke JE, Garcia KC, Grishin NV, Adams PD, Read RJ, Baker D (2021) Accurate prediction of protein structures and interactions using a 3-track network. Science 373(6557): 871–876
Balyschew N, Yushkevich A, Mikirtumov V, Sanchez RM, Sprink T, Kudryashev M (2023) Streamlined structure determination by cryo-electron tomography and subtomogram averaging using TomoBEAR. Nat Commun 14(1): 6543. https://doi.org/10.1038/s41467-023-42085-w
Bassim N, Scott K, Giannuzzi LA (2014) Recent advances in focused ion beam technology and applications. Mater Res Soc Bull 39(4): 317–325
Bayburt TH, Grinkova YV, Sligar SG (2002) Self-assembly of discoidal phospholipid bilayer nanoparticles with membrane scaffold proteins. Nano Lett 2(8): 853–856
Bell JM, Chen M, Durmaz T, Fluty AC, Ludtke SJ (2018) New software tools in EMAN2 inspired by EMDatabank map challenge. J Struct Biol 204(2): 283–290
Bepler T, Morin A, Rapp M, Brasch J, Shapiro L, Noble AJ, Berger B (2019) Positive-unlabeled convolutional neural networks for particle picking in cryo-electron micrographs. Nat Methods 16(11): 1153–1160
Bleck CKE, Merz A, Gutierrez MG, Walther P, Dubochet J, Zuber B, Griffiths G (2010) Comparison of different methods for thin section EM analysis of Mycobacterium smegmatis. J Microsc 237(1): 23–38
Blouin CM, Hamon Y, Gonnord P, Boularan C, Kagan J, Viaris de Lesegno C, Ruez R, Mailfert, S, Bertaux, N, Loew, D, Wunder, C, Johannes, L, Vogt, G, Contreras, F. -X, Marguet D, Casanova J-L, Galès C, He H-T, Lamaze C (2016) Glycosylation-dependent IFN-γR partitioning in lipid and actin nanodomains is critical for JAK activation. Cell 166(4): 920–934
Broadbent L, Depping P, Lodé A, Vaitsopoulou A, Hardy D, Ayub H, Mitchell-White J, Kerr ID, Goddard AD, Bill RM, Rothnie AJ (2022) Detergent-free membrane protein purification using SMA polymer. Methods Mol Biol 2507: 389–404
Browman DT, Hoegg MB, Robbins SM (2007) The SPFH domain-containing proteins: more than lipid raft markers. Trends Cell Biol 17(8): 394–402
Brown DA, Rose JK (1992) Sorting of GPI-anchored proteins to glycolipid-enriched membrane subdomains during transport to the apical cell surface. Cell 68(3): 533–544
Brunet A, Datta SR, Greenberg ME (2001) Transcription-dependent and -independent control of neuronal survival by the PI3K-Akt signaling pathway. Curr Opin Neurobiol 11(3): 297–305
Burt A, Gaifas L, Dendooven T, Gutsche I (2021) A flexible framework for multi-particle refinement in cryo-electron tomography. PLoS Biol 19(8): e3001319. https://doi.org/10.1371/journal.pbio.3001319
Burt A, Toader B, Warshamanage R, von Kügelgen A, Pyle E, Zivanov J, Kimanius D, Bharat TAM, Scheres SHW (2024) An image processing pipeline for electron cryo-tomography in RELION-5. FEBS Open Bio 14(11): 1788–1804
Cao D, Chen M, Zhang R, Wang Z, Huang M, Yu J, Jiang X, Fan Z, Zhang W, Zhou H, Li X, Fu Z, Zhang S, Zheng M (2025) SurfDock is a surface-informed diffusion generative model for reliable and accurate protein–ligand complex prediction. Nat Methods 22(2): 310–322
Casares D, Escribá PV, Rosselló CA (2019) Membrane lipid composition: effect on membrane and organelle structure, function and compartmentalization and therapeutic avenues. Int J Mol Sci 20(9): 2167. https://doi.org/10.3390/ijms20092167
Castaño-Díez D (2017) The Dynamo package for tomography and subtomogram averaging: components for MATLAB, GPU computing and EC2 Amazon Web Services. Acta Crystallogr D Struct Biol 73(Pt 6): 478–487
Chang L Wang F, Connolly K, Meng H, Su Z, Cvirkaite-Krupovic V, Krupovic M, Egelman EH, Si D (2022) DeepTracer-ID: *de novo* protein identification from cryo-EM maps. Biophys J 121(15): 2840–2848
Chavent M, Karia D, Kalli AC, Domański J, Duncan AL, Hedger G, Stansfeld PJ, Seiradake E, Jones EY, Sansom MSP (2018) Interactions of the EphA2 kinase domain with PIPs in membranes: implications for receptor function. Structure 26(7): 1025-1034. e2
Chen J, Zia A, Luo A, Meng H, Wang F, Hou J, Cao R, Si D (2024) Enhancing cryo-EM structure prediction with DeepTracer and AlphaFold2 integration. Brief Bioinform 25(3): bbae118. https://doi.org/10.1093/bib/bbae118
Chen M, Bell JM, Shi X, Sun SY, Wang Z, Ludtke SJ (2019) A complete data processing workflow for cryo-ET and subtomogram averaging. Nat Methods 16(11): 1161–1168
Cheng A, Yu Y (2024) Recent advances in data collection for Cryo-EM methods. Curr Opin Struct Biol 86: 102795. https://doi.org/10.1016/j.sbi.2024.102795
Cheng D, Jenner AM, Shui G, Cheong WF, Mitchell TW, Nealon JR, Kim WS, McCann H, Wenk MR, Halliday GM, Garner B (2011) Lipid pathway alterations in Parkinson's disease primary visual cortex. PLoS One 6(2): e17299. https://doi.org/10.1371/journal.pone.0017299
Ching C, Maufront J, di Cicco A, Lévy D, Dezi M (2024) Cool-contacts: cryo-electron microscopy of membrane contact sites and their components. Contact 7: 1–14
Chuang H, Prescott ED, Kong H, Shields S, Jordt S-E, Basbaum AI, Chao MV, Julius D (2001) Bradykinin and nerve growth factor release the capsaicin receptor from PtdIns(4, 5)P2-mediated inhibition. Nature 411(6840): 957–962
Comet M, Dijkman PM, Boer Iwema R, Franke T, Masiulis S, Schampers R, Raschdorf O, Grollios F, Pryor EE, Drulyte I (2024) Tomo Live: An on-the-fly reconstruction pipeline to judge data quality for cryo-electron tomography workflows. Acta Crystallogr D Struct Biol 80(Pt 4): 247–258

Corum MR, Venkannagari H, Hryc CF, Baker ML (2024) Predictive modeling and cryo-EM: a synergistic approach to modeling macromolecular structure. Biophys J 123(4): 435–450

Coskun Ü, Grzybek M, Drechsel D, Simons K (2011) Regulation of human EGF receptor by lipids. Proc Natl Acad Sci USA, 108(22): 9044–9048

Crofts AR, Hong S, Zhang Z, Berry EA (1999) Physicochemical aspects of the movement of the rieske iron sulfur protein during quinol oxidation by the bc 1 complex from mitochondria and photosynthetic bacteria. Biochemistry 38(48): 15827–15839

Croll TI (2018) ISOLDE: a physically realistic environment for model building into low-resolution electron-density maps. Acta Crystallogr D Struct Biol 74(Pt 6): 519–530

Dahmane S, Kerviel A, Morado DR, Shankar K, Ahlman B, Lazarou M, Altan-Bonnet N, Carlson L-A (2022) Membrane-assisted assembly and selective secretory autophagy of enteroviruses. Nat Commun 13(1): 5986. https://doi.org/10.1038/s41467-022-33483-7

Dar S, Kamerkar SC, Pucadyil TJ (2015) A high-throughput platform for real-time analysis of membrane fission reactions reveals dynamin function. Nat Cell Biol 17(12): 1588–1596

de Saint-Jean M, Delfosse V, Douguet D, Chicanne G, Payrastre B, Bourguet W, Antonny B, Drin G (2011) Osh4p exchanges sterols for phosphatidylinositol 4-phosphate between lipid bilayers. J Cell Biol 195(6): 965–978

Denisov IG, Sligar SG (2016) Nanodiscs for structural and functional studies of membrane proteins. Nat Struct Mol Biol 23(6): 481–486

Denisov IG, Sligar SG (2017) Nanodiscs in membrane biochemistry and biophysics. Chem Rev, 117(6): 4669–4713

Denisov IG, Sligar SG (2024) Nanodiscs for the study of membrane proteins. Curr Opin Struct Biol 87: 102844. https://doi.org/10.1016/j.sbi.2024.102844

Ding G, Liu Y, Zhang R, Xin HL (2019) A joint deep learning model to recover information and reduce artifacts in missing-wedge sinograms for electron tomography and beyond. Sci Rep 9(1): 12803. https://doi.org/10.1038/s41598-019-49267-x

Dong YY, Pike ACW, Mackenzie A, McClenaghan C, Aryal P, Dong L, Quigley A, Grieben M, Goubin S, Mukhopadhyay S, Ruda GF, Clausen MV, Cao L, Brennan PE, Burgess-Brown NA, Sansom MSP, Tucke, SJ, Carpenter EP (2015) K2P channel gating mechanisms revealed by structures of TREK-2 and a complex with Prozac. Science 347(6227): 1256–1259

Dowhan W, Vitrac H, Bogdanov M (2019) Lipid-assisted membrane protein folding and topogenesis. Protein J 38(3): 274–288

Doyle MT, Jimah JR, Dowdy T, Ohlemacher SI, Larion M, Hinshaw JE, Bernstein HD (2022) Cryo-EM structures reveal multiple stages of bacterial outer membrane protein folding. Cell 185(7): 1143–1156

Du DX, Fitzpatrick AWP (2023) Design of an ultrafast pulsed ponderomotive phase plate for cryo-electron tomography. Cell Rep Methods 3(1): 100387. https://doi.org/10.1016/j.crmeth.2022.100387

Dutta M, Acharya P (2024) Cryo-electron microscopy in the study of virus entry and infection. Front Mol Biosci 11: 1429180. https://doi.org/10.3389/fmolb.2024.1429180

Eisenstein F, Yanagisawa H, Kashihara H, Kikkawa M, Tsukita S, Danev R (2023) Parallel cryo electron tomography on *in situ* lamellae. Nat Methods 20(1): 131–138

Emsley P, Lohkamp B, Scott WG, Cowtan K (2010) Features and development of Coot. Acta Crystallogr D Biol Crystallogr 66(Pt 4): 486–501

Fabelo N, Martín V, Marín R, Moreno D, Ferrer I, Díaz M (2014) Altered lipid composition in cortical lipid rafts occurs at early stages of sporadic Alzheimer's disease and facilitates APP/BACE1 interactions. Neurobiol Aging 35(8): 1801–1812

Faelber K, Posor Y, Gao S, Held M, Roske Y, Schulze D, Haucke V, Noé F, Daumke O (2011) Crystal structure of nucleotide-free dynamin. Nature 477(7366): 556–560

Fahy E, Subramaniam S, Brown HA, Glass CK, Merrill AH, Murphy RC, Raetz CRH, Russell DW, Seyama Y, Shaw W, Shimizu T, Spener F, Van Meer G, VanNieuwenhze MS, White SH, Witztum JL, Dennis EA (2005) A comprehensive classification system for lipids. J Lipid Res 46(5): 839–861

Fan X, Zhao L, Liu C, Zhang J-C, Fan K, Yan X, Peng H-L, Lei J, Wang H-W (2017) Near-atomic resolution structure determination in over-focus with volta phase plate by Cs-corrected cryo-EM. Structure 25(10): 1623-1630. e3

Feng Z, Alvarenga OE, Accardi A (2024) Structural basis of closed groove scrambling by a TMEM16 protein. Nat Struct Mol Biol 31(10): 1468–1481

Ferguson SM, De Camilli P (2012) Dynamin, a membrane-remodelling GTPase. Nat Rev Mol Cell Biol 13(2): 75–88

Fernandez J-J, Li S (2021) TomoAlign: a novel approach to correcting sample motion and 3D CTF in CryoET. J Struct Biol 213(4): 107778. https://doi.org/10.1016/j.jsb.2021.107778

Flanagan DJ, Woodcock SA, Phillips C, Eagle C, Sansom OJ (2022) Targeting ligand-dependent wnt pathway dysregulation in gastrointestinal cancers through porcupine inhibition. Pharmacol Ther 238: 108179. https://doi.org/10.1016/j.pharmthera.2022.108179

Förster F (2022) Subtomogram analysis: the sum of a tomogram's particles reveals molecular structure *in situ*. J Struct Biol X 6: 100063. https://doi.org/10.1016/j.yjsbx.2022.100063

Fratti RA (2021) Editorial: effects of membrane lipids on protein function. Front Cell Dev Biol 9: 675264. https://doi.org/10.3389/fcell.2021.675264

Frederik PM, Hubert DHW (2005) Cryoelectron microscopy of liposomes. Methods Enzymol 391: 431–448

Frick M, Bright NA, Riento K, Bray A, Merrified C, Nichols BJ (2007) Coassembly of flotillins induces formation of membrane microdomains, membrane curvature, and vesicle budding. Curr Biol 17(13): 1151–1156

Fu Z, MacKinnon R (2024) Structure of the flotillin complex in a native membrane environment. Proc Natl Acad Sci USA 121(29): e2409334121. https://doi.org/10.1073/pnas.2409334121

George B, Assaiya A, Roy RJ, Kembhavi A, Chauhan R, Paul G, Kumar J, Philip NS (2021) CASSPER is a semantic segmentation-based particle picking algorithm for single-particle cryo-electron microscopy. Commun Biol 4(1): 200. https://doi.org/10.1038/s42003-021-01721-1

Giri N, Cheng J (2024) *De novo* atomic protein structure modeling for cryoEM density maps using 3D transformer and HMM. Nat Commun 15(1): 5511. https://doi.org/10.1038/s41467-024-49647-6

Glukhov G, Karlova M, Kravchuk E, Glukhova A, Trifonova E, Sokolova OS (2024) Purification of potassium ion channels using styrene-maleic acid copolymers. Methods Mol Biol 2796: 73–86

Griffiths G, Lucocq JM (2014) Antibodies for immunolabeling by light and electron microscopy: not for the faint hearted. Histochem Cell Biol 142(4): 347–360

Guo YR, MacKinnon R (2017) Structure-based membrane dome mechanism for Piezo mechanosensitivity. eLife 6: e33660. https://doi.org/10.7554/eLife.33660

Hagen WJH, Wan W, Briggs JAG (2017) Implementation of a cryo-electron tomography tilt-scheme optimized for high resolution subtomogram averaging. J Struct Biol 197(2): 191–198

Han R, Wan X, Wang Z, Hao Y, Zhang J, Chen Y, Gao X, Liu Z, Ren F,

Sun F, Zhang F (2017) AuTom: a novel automatic platform for electron tomography reconstruction. J Struct Biol 199(3): 196–208

Han Y, Zhou Z, Jin R, Dai F, Ge Y, Ju X, Ma X, He S, Yuan L, Wang Y, Yang W, Yue X, Chen Z, Sun Y, Corry B, Cox CD, Zhang Y (2024) Mechanical activation opens a lipid-lined pore in OSCA ion channels. Nature 628(8009): 910–918

Haselwandter C, Guo YR, Fu Z, MacKinnon R (2022) Elastic properties and shape of the Piezo dome underlying its mechanosensory function. Proc Natl Acad Sci USA 119(40): e2208034119. https://doi.org/10.1073/pnas.2208034119

Haselwandter CA, MacKinnon R (2018) Piezo's membrane footprint and its contribution to mechanosensitivity. eLife 7: e41968. https://doi.org/10.7554/eLife.41968

He J, Huang S-Y (2021) EMNUSS: a deep learning framework for secondary structure annotation in cryo-EM maps. Brief Bioinform 22(6): bbab156. https://doi.org/10.1093/bib/bbab156

He J, Lin P, Chen J, Cao H, Huang S-Y (2022) Model building of protein complexes from intermediate-resolution cryo-EM maps with deep learning-guided automatic assembly. Nat Commun 13(1): 4066. https://doi.org/10.1038/s41467-022-31748-9

He XH, Li JR, Shen SY, Xu HE (2025) AlphaFold3 versus experimental structures: assessment of the accuracy in ligand-bound G protein-coupled receptors. Acta Pharmacol Sin 46(4): 1111–1122

Heimowitz A, Andén J, Singer A (2018) APPLE picker: automatic particle picking, a low-effort cryo-EM framework. J Struct Biol 204(2): 215–227

Hein C, Henrich E, Orbán E, Dötsch V, Bernhard F (2014) Hydrophobic supplements in cell -free systems: designing artificial environments for membrane proteins. Eng Life Sci 14(4): 365–379

Herbert FC, Abeyrathna SS, Abeyrathna NS, Wijesundara YH, Brohlin OR, Luzuriaga MA, Durand-Silva A, Diwakara SD, Smaldone RA, Meloni G, Gassensmith JJ (2021) Stabilization of supramolecular membrane protein–lipid bilayer assemblies through immobilization in a crystalline exoskeleton. Nat Commun 12(1): 2202. https://doi.org/10.1038/s41467-021-22285-y

Hilgemann DW, Feng S, Nasuhoglu C (2001) The complex and intriguing lives of PIP2 with ion channels and transporters. Sci STKE 2001(111): re19. https://doi.org/10.1126/stke.2001.111.re19

Lee HS, Youn T, Byrne B, Chae PS (2022) Impact of novel detergents on membrane protein studies. Chem 8: 980–1013

Hoang Trinh TK, Catalano C, Guo Y (2023) Fabrication of membrane proteins in the form of native cell membrane nanoparticles using novel membrane active polymers. Nanoscale Adv 5(21): 5932–5940

Hosokawa M, Inaba M, Tanaka M, Ogawara K-I (2024) Uptake pathway of styrene maleic acid copolymer-coated lipid emulsions under acidic tumor microenvironment. J Pharm Sci 113(4): 1047–1053

Hsieh C, Schmelzer T, Kishchenko G, Wagenknecht T, Marko M (2014) Practical workflow for cryo focused-ion-beam milling of tissues and cells for cryo-TEM tomography. J Struct Biol 185(1): 32–41

Huang L, Cobessi D, Tung EY, Berry EA (2005) Binding of the respiratory chain inhibitor antimycin to the mitochondrial bc1 complex: a new crystal structure reveals an altered intramolecular hydrogen-bonding pattern. J Mol Biol 351(3): 573–597

Iancu CV, Tivol WF, Schooler JB, Dias DP, Henderson GP, Murphy GE, Wright ER, Li Z, Yu Z, Briegel A, Gan, L, He Y, Jensen GJ (2006) Electron cryotomography sample preparation using the Vitrobot. Nat Protoc 1(6): 2813–2819

Ikonen E, Zhou X (2021) Cholesterol transport between cellular membranes: a balancing act between interconnected lipid fluxes. Dev Cell 56(10): 1430–1436

Inagaki S, Ghirlando R, Grisshammer R (2013) Biophysical characterization of membrane proteins in nanodiscs. Methods (San Diego, Calif.) 59(3): 287–300

Iversen L, Mathiasen S, Larsen JB, Stamou D (2015) Membrane curvature bends the laws of physics and chemistry. Nat Chem Biol 11(11): 822–825

Jakobi AJ, Wilmanns M, Sachse C (2017) Model-based local density sharpening of cryo-EM maps. eLife, 6: e27131. https://doi.org/10.7554/eLife.27131

Jamali K, Käll L, Zhang R, Brown A, Kimanius D, Scheres SHW (2024) Automated model building and protein identification in cryo-EM maps. Nature 628(8007): 450–457

Jimah JR, Kundu N, Stanton AE, Sochacki KA, Canagarajah B, Chan L, Strub M-P, Wang H, Taraska JW, Hinshaw JE (2024) Cryo-EM structures of membrane-bound dynamin in a post-hydrolysis state primed for membrane fission. Dev Cell 59(14): 1783-1793. e5

Jojoa-Cruz S, Saotome K, Murthy SE, Tsui CCA, Patapoutian A (2018) Cryo-EM structure of the mechanically activated ion channel OSCA1.2. eLife 7: e41845. doi: 10.7554/eLife.41845

Jost PC, Griffith OH, Capaldi RA, Vanderkooi G (1973) Evidence for boundary lipid in membranes. Proc Natl Acad Sci USA 70(2): 480–484

Jumper J, Evans R, Pritzel A, Green T, Figurnov M, Ronneberger O, Tunyasuvunakool K, Bates R, Žídek A, Potapenko A, Bridgland A, Meyer C, Kohl SAA, Ballard AJ, Cowie A, Romera-Paredes B, Nikolov S, Jain R, Adler J, Back T, Petersen S, Reiman D, Clancy E, Zielinski M, Steinegger M, Pacholska M, Berghammer T, Bodenstein S, Silver D, Vinyals O, Senior AW, Kavukcuoglu K, Kohli P, Hassabis D (2021) Highly accurate protein structure prediction with AlphaFold. Nature 596(7873): 583–589

Karanth S, Benthin J, Wiesenfarth M, Somoza V, Koehler M (2024) Nanodisc technology: direction toward physicochemical characterization of chemosensory membrane proteins in food flavor research. J Agric Food Chem 72(26): 14521–14529

Karelina M, Noh JJ, Dror RO (2023) How accurately can one predict drug binding modes using AlphaFold models? eLife 12: RP89386. doi: 10.7554/eLife.89386

Karimi R, Coupland CE, Rubinstein JL (2024) Vesicle Picker: a tool for efficient identification of membrane protein complexes in vesicles. J Struct Biol 216(4): 108148. https://doi.org/10.1016/j.jsb.2024.108148

Kaur S, Gomez-Blanco J, Khalifa AAZ, Adinarayanan S, Sanchez-Garcia R, Wrapp D, McLellan JS, Bui KH, Vargas J (2021) Local computational methods to improve the interpretability and analysis of cryo-EM maps. Nat Commun 12(1): 1240. https://doi.org/10.1038/s41467-021-21509-5

Keller, J, & Fernández-Busnadiego, R. (2024). *In situ* studies of membrane biology by cryo-electron tomography. Current Opinion in Cell Biology, 88: 102363. doi: 10.1038/s41467-021-21509-5

Kelley K, Raczkowski AM, Klykov O, Jaroenlak P, Bobe D, Kopylov M, Eng ET, Bhabha G, Potter CS, Carragher B, Noble AJ (2022) Waffle Method: a general and flexible approach for improving throughput in FIB-milling. Nat Commun 13(1): 1857. https://doi.org/10.1038/s41467-022-29501-3

Khavnekar S, Erdmann PS, Wan W (2024) TOMOMAN: a software package for large-scale cryo-electron tomography data preprocessing, community data sharing and collaborative

computing. J Appl Crystallogr 57(Pt 6): 2010–2016
Klein S, Cortese M, Winte, SL, Wachsmuth-Melm M, Neufeldt CJ, Cerikan B, Stanifer ML, Boulant S, Bartenschlager R, Chlanda P (2020) SARS-CoV-2 structure and replication characterized by *in situ* cryo-electron tomography. Nat Commun 11(1): 5885. https://doi.org/10.1038/s41467-020-19619-7
Klein S, Golani G, Lolicato F, Lahr C, Beyer D, Herrmann A, Wachsmuth-Melm M, Reddmann N, Brecht R, Hosseinzadeh M, Kolovou A, Makroczyova J, Peterl S, Schorb M, Schwab Y, Brügger B, Nickel W, Schwarz US, Chlanda P (2023) IFITM3 blocks influenza virus entry by sorting lipids and stabilizing hemifusion. Cell Host Microbe 31(4): 616-633. e20
Klykov O, Bobe D, Paraan M, Johnston JD, Potter CS, Carragher B, Kopylov M, Noble AJ (2022) *In situ* cryo-FIB/SEM specimen preparation using the Waffle Method. Bio Protoc 12(21): e4544. https://doi.org/10.21769/BioProtoc.4544
Koh A, Khavnekar S, Yang W, Karia D, Cats D, van der Ploeg R, Grollios F, Raschdorf O, Kotecha A, Němeček D (2022) Routine collection of high-resolution cryo-EM datasets using 200 kV transmission electron microscope. J Vis Exp 16: (181)). https://doi.org/10.3791/63519
Kong L, Sochacki K A, Wang H, Fang S, Canagarajah B, Keh, AD, Rice WJ, Strub M-P, Taraska JW, Hinshaw JE (2018) Cryo-EM of the dynamin polymer assembled on lipid membrane. Nature 560(7717): 258–262
Kopf AH, Dörr JM, Koorengevel MC, Antoniciello F, Jahn H, Killian JA (2020) Factors influencing the solubilization of membrane proteins from *Escherichia coli* membranes by styrene-maleic acid copolymers. Biochim Biophys Acta Biomembr 1862(2): 183125. https://doi.org/10.1016/j.bbamem.2019.183125
Krapp LF, Abriata LA, Cortés Rodriguez F, Dal Peraro M (2023) PeSTo: parameter-free geometric deep learning for accurate prediction of protein binding interfaces. Nat Commun 14(1): 2175. https://doi.org/10.1038/s41467-023-37701-8
Kremer JR, Mastronarde DN, McIntosh JR (1996) Computer visualization of three-dimensional image data using IMOD. J Struct Biol 116(1): 71–76
Krishnarjuna B, Ramamoorthy A (2022) Detergent-free isolation of membrane proteins and strategies to study them in a near-native membrane environment. Biomolecules 12(8): 1076. https://doi.org/10.3390/biom12081076
Kuba J, Mitchels J, Hovorka M, Erdmann P, Berka L, Kirmse R, KÖnig J, DE Bock J, Goetze B, Rigort A (2021) Advanced cryo-tomography workflow developments—correlative microscopy, milling automation and cryo-lift-out. J Microsc 281(2): 112–124
Lajoie P, Nabi IR (2010) Lipid rafts, caveolae, and their endocytosis. Int Rev Cell Mol Biol 282: 135–163
Lapatsina L, Brand J, Poole K, Daumke O, Lewin GR (2012) Stomatin-domain proteins. Eur J Cell Biol, 91(4): 240–245
Li P-N, Oliveira SHP de, Wakatsuki S, Bedem H van den (2020) Sequence-guided protein structure determination using graph convolutional and recurrent networks. arXiv. https://doi.org/10.48550/arXiv.2007.06847
Li S, Jia X, Niu T, Zhang X, Qi C, Xu W, Deng H, Sun F, Ji G (2023a) HOPE-SIM, a cryo-structured illumination fluorescence microscopy system for accurately targeted cryo-electron tomography. Commun Biol 6(1): 474. https://doi.org/10.1038/s42003-023-04850-x
Li S, Wang Z, Jia X, Niu T, Zhang J, Yin G, Zhang X, Zhu Y, Ji G, Sun F (2023b) ELI trifocal microscope: A precise system to prepare target cryo-lamellae for *in situ* cryo-ET study. Nat Methods 20(2): 276–283
Liedtke J, Depelteau JS, Briegel A (2022) How advances in cryo-electron tomography have contributed to our current view of bacterial cell biology. J Struct Biol X 6: 100065. https://doi.org/10.1016/j.yjsbx.2022.100065
Lige T, Wang L (2020) Cryo-EM sample preparation method for extremely low concentration liposomes. Ultramicroscopy 208: 112849. https://doi.org/10.1016/j.ultramic.2019.112849
Lin BJ, Tsao SH, Chen A, Hu SK, Chao L, Chao PG (2017) Lipid rafts sense and direct electric field-induced migration. Proc Natl Acad Sci USA 114(32): 8568–8573
Lin Y-C, Guo YR, Miyagi A, Levring J, MacKinnon R, Scheuring S (2019) Force-induced conformational changes in PIEZO1. Nature 573(7773): 230–234
Lingwood D, Simons K (2010) Lipid rafts as a membrane-organizing principle. Science 327(5961): 46–50
Liu D, Liman ER (2003) Intracellular Ca^{2+} and the phospholipid PIP2 regulate the taste transduction ion channel TRPM5. Proc Natl Acad Sci USA 100(25): 15160–15165
Liu J, Alvarez FJD, Clare DK, Noel JK, Zhang P (2021) CryoEM structure of the super-constricted two-start dynamin 1 filament. Nat Commun 12(1): 5393. https://doi.org/10.1038/s41467-021-25741-x
Liu X, Wang J, Sun L (2018) Structure of the hyperosmolality-gated calcium-permeable channel OSCA1.2. Nat Commun 9(1): 5060. doi: 10.1038/s41467-018-07564-5
Liu Y-T, Zhang H, Wang H, Tao C-L, Bi G-Q, Zhou ZH (2022) Isotropic reconstruction for electron tomography with deep learning. Nat Commun 13(1): 6482. https://doi.org/10.1038/s41467-022-33957-8
Long DM, Singh MK, Small KA, Watt J (2022) Cryo-FIB for TEM investigation of soft matter and beam sensitive energy materials. Nanotechnology 33(50): 503001. https://doi.org/10.1088/1361-6528/ac92eb
Lu W, Zhang J, Huang W, Zhang Z, Jia X, Wang Z, Shi L, Li C, Wolynes PG, Zheng S (2024) DynamicBind: predicting ligand-specific protein-ligand complex structure with a deep equivariant generative model. Nat Commun 15(1): 1071. https://doi.org/10.1038/s41467-024-45461-2
Ma C, Wang C, Luo D, Yan L, Yang W, Li N, Gao N (2022) Structural insights into the membrane microdomain organization by SPFH family proteins. Cell Res 32(2): 176–189
Mahamid J, Pfeffer S, Schaffer M, Villa E, Danev R, Kuhn Cuellar L, Förster F, Hyman AA, Plitzko JM, Baumeister W (2016) Visualizing the molecular sociology at the HeLa cell nuclear periphery. Science 351(6276): 969–972
Mahamid J, Schampers R, Persoon H, Hyman AA, Baumeister W, Plitzko JM (2015) A focused ion beam milling and lift-out approach for site-specific preparation of frozen-hydrated lamellas from multicellular organisms. J Struct Biol 192(2): 262–269
Marko M, Hsieh C, Schalek R, Frank J, Mannella C (2007) Focused-ion-beam thinning of frozen-hydrated biological specimens for cryo-electron microscopy. Nat Methods 4(3): 215–217
Marsh D (2007) Lateral pressure profile, spontaneous curvature frustration, and the incorporation and conformation of proteins in membranes. Biophys J 93(11): 3884–3899
Mastronarde DN, Held SR (2017) Automated tilt series alignment and tomographic reconstruction in IMOD. J Struct Biol 197(2): 102–113
McMahon HT, Boucrot E (2015) Membrane curvature at a glance. J Cell Sci 128(6): 1065–1070
McMullan G, Faruqi AR, Henderson R (2016) Direct electron detectors. Methods Enzymol 579: 1–17
Mendez JH, Mehrani A, Randolph P, Stagg S (2019) Throughput and resolution with a next-generation direct electron detector. IUCrJ 6(6): 1007–1013
Meyer zu Heringdorf D, Jakobs KH (2007) Lysophospholipid

receptors: signalling, pharmacology and regulation by lysophospholipid metabolism. Biochim Biophys Acta 1768(4): 923–940

Mileykovskaya E, Dowhan W (2014) Cardiolipin-dependent formation of mitochondrial respiratory supercomplexes. Chem Phys Lipids 179: 42–48

Mo ML, Li MR, Chen Z, Liu XW, Sheng Q, Zhou HM (2013) Inhibition of the Wnt palmitoyltransferase porcupine suppresses cell growth and downregulates the Wnt/beta-catenin pathway in gastric cancer. Oncol Lett 5(5): 1719–1723

Moor H, Bellin G, Sandri C, Akert K (1980) The influence of high pressure freezing on mammalian nerve tissue. Cell Tissue Res 209(2): 201–216

Mostosi P, Schindelin H, Kollmannsberger P, Thorn A (2020) Haruspex: a neural network for the automatic identification of oligonucleotides and protein secondary structure in cryo - electron microscopy maps. Angew Chem Int Ed Engl 59(35): 14788–14795

Mu Q, Deng H, An X, Liu G, Liu C (2024) Designing nanodiscs as versatile platforms for on-demand therapy. Nanoscale 16(5): 2220–2234

Murthy SE, Dubin AE, Whitwam T, Jojoa-Cruz S, Cahalan SM, Mousavi SAR, Ward AB, Patapoutian A (2018) OSCA/TMEM63 are an evolutionarily conserved family of mechanically activated ion channels. eLife, 7: e41844. https://doi.org/10.7554/eLife.41844

Natesan V, Kim SJ (2021) Diabetic nephropathy—a review of risk factors, progression, mechanism, and dietary management. Biomol Ther (Seoul) 29(4): 365–372

Ni T, Frosio T, Mendonça L, Sheng Y, Clare D, Himes BA, Zhang P (2022) High-resolution *in situ* structure determination by cryo-electron tomography and subtomogram averaging using emClarity. Nat Protoc, 17(2): 421–444

Nsairat H, Khater D, Sayed U, Odeh F, Al Bawab A, Alshaer W (2022) cccc. Heliyon 8(5): e09394. https://doi.org/10.1016/j.heliyon.2022.e09394

Oates J, Watts A (2011) Uncovering the intimate relationship between lipids, cholesterol and GPCR activation. Curr Opin Struct Biol 21(6): 802–807

Orekhov PS, Bozdaganyan ME, Voskoboynikova N, Mulkidjanian AY, Karlova MG, Yudenko A, Remeeva A, Ryzhykau YL, Gushchin I, Gordeliy VI, Sokolova OS, Steinhoff H-J, Kirpichnikov MP, Shaitan KV (2022. Mechanisms of formation, structure, and dynamics of lipoprotein discs stabilized by amphiphilic copolymers: a comprehensive review. Nanomaterials (Basel) 12(3): 361. doi: 10.3390/nano12030361

Özhan G, Sezgin E, Wehner D, Pfister AS, Kühl SJ, Kagermeier-Schenk B, Kühl M, Schwille P, Weidinger G (2013) Lypd6 enhances Wnt/β-catenin signaling by promoting Lrp6 phosphorylation in raft plasma membrane domains. Dev Cell 26(4): 331–345

Padmanabha Das KM, Shih WM, Wagner G, Nasr ML (2020) Large nanodiscs: a potential game changer in structural biology of membrane protein complexes and virus entry. Front Bioeng Biotechnol 8: 539. https://doi.org/10.3389/fbioe.2020.00539

Pang X, Zhang Y, Park K, Liao Z, Li J, Xu J, Hong M-T, Yin G, Zhang T, Wang Y, Egelman EH, Fan J, Park S-Y, Hsu VW, Sun F (2023) Structural elucidation of how ARF small GTPases induce membrane tubulation for vesicle fission. bioRxiv. doi: 10.1101/2023.12.19.572083

Parkhurst JM, Varslot T, Dumoux M, Siebert CA, Darrow M, Basham M, Kirkland A, Grange M, Evans G, Naismith JH (2024) Pillar data-acquisition strategies for cryo-electron tomography of beam-sensitive biological samples. Acta Crystallogr D Struct Biol 80(Pt 6): 421–438

Peng R, Fu X, Mendez JH, Randolph PS, Bammes BE, Stagg SM, Li X (2023) Characterizing the resolution and throughput of the Apollo direct electron detector. J Struct Biol X 7: 100080. https://doi.org/10.1016/j.yjsbx.2022.100080

Pettersen JM, Yang Y, Robinson AS (2023) Advances in nanodisc platforms for membrane protein purification. Trends Biotechnol 41(8): 1041–1054

Pfab J, Phan NM, Si D (2021) DeepTracer for fast *de novo* cryo-EM protein structure modeling and special studies on CoV-related complexes. Proc Natl Acad Sci USA 118(2): e2017525118. https://doi.org/10.1073/pnas.2017525118

Phillips GR, Hancock SE, Brown SHJ, Jenner AM, Kreilaus F, Newell KA, Mitchell TW (2020) Cholesteryl ester levels are elevated in the caudate and putamen of Huntington's disease patients. Sci Rep 10(1): 20314. https://doi.org/10.1038/s41598-020-76973-8

Pöge M, Mahamid J, Imanishi SS, Plitzko JM, Palczewski K, Baumeister W (2021) Determinants shaping the nanoscale architecture of the mouse rod outer segment. eLife 10: e72817. https://doi.org/10.7554/eLife.72817

Polley A, Orłowski A, Danne R, Gurtovenko AA, Bernardino de la Serna J, Eggeling C, Davis SJ, Róg T, Vattulainen I (2017) Glycosylation and lipids working in concert direct CD2 ectodomain orientation and presentation. J Phys Chem Lett 8(5): 1060–1066

Pozza A, Giraud F, Cece Q, Casiraghi M, Point E, Damian M, Le Bon C, Moncoq K, Banères J-L, Lescop E, Catoire LJ (2022) Exploration of the dynamic interplay between lipids and membrane proteins by hydrostatic pressure. Nat Commun 13(1): 1780. https://doi.org/10.1038/s41467-022-29410-5

Puri V, Watanabe R, Dominguez M, Sun X, Wheatley CL, Marks DL, Pagano RE (1999) Cholesterol modulates membrane traffic along the endocytic pathway in sphingolipid-storage diseases. Nat Cell Biol 1(6): 386–388

Qiu W, Fu Z, Xu GG, Grassucci RA, Zhang Y, Frank J, Hendrickson WA, Guo Y (2018) Structure and activity of lipid bilayer within a membrane-protein transporter. Proc Natl Acad Sci USA 115(51): 12985–12990

Rahman MdM, Teng J, Worrell BT, Noviello CM, Lee M, Karlin A, Stowell MHB, Hibbs RE (2020) Structure of the native muscle-type nicotinic receptor and inhibition by snake venom toxins. Neuron 106(6): 952-962. e5

Ramírez-Aportela E, Vilas JL, Glukhova A, Melero R, Conesa P, Martínez M, Maluenda D, Mota J, Jiménez A, Vargas J, Marabini R, Sexton PM, Carazo JM, Sorzano COS (2020) Automatic local resolution-based sharpening of cryo-EM maps. Bioinformatics 36(3): 765–772

Real Hernandez LM, Levental I (2023) Lipid packing is disrupted in copolymeric nanodiscs compared with intact membranes. Biophys J 122(11): 2256–2266

Riento K, Frick M, Schafer I, Nichols BJ (2009) Endocytosis of flotillin-1 and flotillin-2 is regulated by Fyn kinase. J Cell Sci 122(Pt 7): 912–918

Rigaud J-L, Lévy D (2003) Reconstitution of membrane proteins into liposomes. Methods Enzymol 372: 65–86

Rigort A, Plitzko JM (2015) Cryo-focused-ion-beam applications in structural biology. Arch Biochem Biophys 581: 122–130

Rosenthal P, Henderson R (2003) Optimal determination of particle orientation, absolute hand, and contrast loss in single-particle electron cryomicroscopy. J Mol Biol 333(4): 721–745

Rouck JE, Krapf JE, Roy J, Huff HC, Das A (2017) Recent advances in nanodisc technology for membrane protein studies (2012-2017). FEBS Lett 591(14): 2057–2088

Ruiz Caridad A, Erni R, Vogel A, Rossell MD (2022) Applications of a novel electron energy filter combined with a hybrid-pixel

direct electron detector for the analysis of functional oxides by STEM/EELS and energy-filtered imaging. Micron 160: 103331. https://doi.org/10.1016/j.micron.2022.103331

Sanchez-Garcia R, Gomez-Blanco J, Cuervo A, Carazo JM, Sorzano COS, Vargas J (2021) DeepEMhancer: a deep learning solution for cryo-EM volume post-processing. Commun Biol 4(1): 874. https://doi.org/10.1038/s42003-021-02399-1

Saotome K, Murthy SE, Kefauver JM, Whitwam T, Patapoutian A, Ward AB (2018) Structure of the mechanically activated ion channel Piezo1. Nature, 554(7693): 481–486

Sawczyc H, Heit S, Watts A (2023) A comparative characterisation of commercially available lipid-polymer nanoparticles formed from model membranes. Eur Biophys J 52(1-2): 39–51

Scardino V, Di Filippo JI, Cavasotto CN (2023. How good are AlphaFold models for docking-based virtual screening? iScience 26(1): 105920. doi: 10.1016/j.isci.2022.105920

Schaffer M, Pfeffer S, Mahamid J, Kleindiek S, Laugks T, Albert S, Engel BD, Rummel A, Smith AJ, Baumeister W, Plitzko JM (2019) A cryo-FIB lift-out technique enables molecular-resolution cryo-ET within native Caenorhabditis elegans tissue. Nat Methods 16(8): 757–762

Scheyer MW, Campbell C, William PL, Hussain M, Begum A, Fonseca SE, Asare IK, Dabney P, Dabney-Smith C, Lorigan GA, Sahu ID (2023) Electron paramagnetic resonance spectroscopic characterization of the human KCNE3 protein in lipodisq nanoparticles for structural dynamics of membrane proteins. Biophys Chem 301: 107080. https://doi.org/10.1016/j.bpc.2023.107080

Schmidpeter PA, Nimigean CM (2021) Correlating ion channel structure and function. Methods Enzymol 652: 3–30

Schorb M, Haberbosch I, Hagen WJH, Schwab Y, Mastronarde DN (2019) Software tools for automated transmission electron microscopy. Nat Methods 16(6): 471–477

Sexton DL, Burgold S, Schertel A, Tocheva EI (2022) Super-resolution confocal cryo-CLEM with cryo-FIB milling for *in situ* imaging of Deinococcus radiodurans. Curr Res Struct Biol 4: 1–9

Sezgin E, Azbazdar Y, Ng XW, Teh C, Simons K, Weidinger G, Wohland T, Eggeling C, Ozhan G (2017) Binding of canonical Wnt ligands to their receptor complexes occurs in ordered plasma membrane environments. FEBS J 284(15): 2513–2526

Sheng Y, Morris K, Radecke J, Zhang P (2022) Cryo-electron tomography remote data collection and subtomogram averaging. J Vis Exp 185. doi: 10.3791/63923

Si D, Moritz SA, Pfab J, Hou J, Cao R, Wang L, Wu T, Cheng J (2020). Deep learning to predict protein backbone structure from high-resolution cryo-EM density maps. Sci Rep 10(1): 4282. doi: 10.1038/s41598-020-60598-y

Skarda L, Kowal J, Locher KP (2021) Structure of the human cholesterol transporter ABCG1. J Mol Biol 433(21): 167218. https://doi.org/10.1016/j.jmb.2021.167218

Song K, Awata J, Tritschler D, Bower R, Witman GB, Porter ME, Nicastro D (2015) *In situ* localization of N and C termini of subunits of the flagellar nexin-dynein regulatory complex (N-DRC) using SNAP tag and cryo-electron tomography. J Biol Chem 290(9): 5341–5353

Spehner D, Steyer AM, Bertinetti L, Orlov I, Benoit L, Pernet-Gallay K, Schertel A, Schultz P (2020) Cryo-FIB-SEM as a promising tool for localizing proteins in 3D. J Struct Biol 211(1): 107528. https://doi.org/10.1016/j.jsb.2020.107528

Strickland KM, Neselu K, Grant AJ, Espy CL, McCarty NA, Schmidt-Krey I (2021) Reconstitution of detergent-solubilized membrane proteins into proteoliposomes and nanodiscs for functional and structural studies. Methods Mol Biol 2302: 21–35

Su B, Huang K, Peng Z, Amunts A, Yang J (2024) Improved automated model building for cryo-EM maps using CryFold. bioRxiv. https://doi.org/10.1101/2024.11.13.623164

Suh BC, Hille B (2005) Regulation of ion channels by phosphatidylinositol 4, 5-bisphosphate. Curr Opin Neurobiol 15(3): 370–378

Sun F, Zhang X, Zhang K (2023) New frontier of cryo-electron microscopy technology. J Mol Biol 435(9): 168098. https://doi.org/10.1016/j.jmb.2023.168098

Sundborger AC, Fang S, Heymann JA, Ray P Chappie JS, Hinshaw JE (2014) A dynamin mutant defines a superconstricted prefission state. Cell Rep 8(3): 734–742

Sweitzer SM, Hinshaw JE (1998) Dynamin undergoes a GTP-dependent conformational change causing vesiculation. Cell 93(6): 1021–1029

Tai L, Zhu Y, Ren H, Huang X, Zhang C, Sun F (2022) 8 Å structure of the outer rings of the Xenopus laevis nuclear pore complex obtained by cryo-EM and AI. Protein Cell 13(10): 760–777

Takei K, McPherson PS, Schmid SL, Camilli PD (1995) Tubular membrane invaginations coated by dynamin rings are induced by GTP-γS in nerve terminals. Nature 374(6518): 186–190

Tao X, Zhao C, MacKinnon R (2023) Membrane protein isolation and structure determination in cell-derived membrane vesicles. Proc Natl Acad Sci USA 120(18): e2302325120. https://doi.org/10.1073/pnas.2302325120

Tavernarakis N, Driscoll M, Kyrpides NC (1999) The SPFH domain: implicated in regulating targeted protein turnover in stomatins and other membrane-associated proteins. Trends Biochem Sci 24(11): 425–427

Tegunov D, Cramer P (2019) Real-time cryo-electron microscopy data preprocessing with Warp. Nat Methods 16(11): 1146–1152

Tegunov D, Xue L, Dienemann C, Cramer P, Mahamid J (2021) Multi-particle cryo-EM refinement with M visualizes ribosome-antibiotic complex at 3.5 Å in cells. Nat Methods, 18(2): 186–193

Terwilliger TC (2000) Maximum-likelihood density modification. Acta Crystallogr D Biol Crystallogr 56(8): 965–972

Terwilliger TC, Ludtke SJ, Read RJ, Adams PD, Afonine PV (2020a) Improvement of cryo-EM maps by density modification. Nat Methods 17(9): 923–927

Terwilliger TC, Sobolev OV, Afonine PV, Adams PD (2018) Automated map sharpening by maximization of detail and connectivity. Acta Crystallogr D Struct Biol 74(Pt 6): 545–559

Terwilliger TC, Sobolev OV, Afonine PV, Adams PD, Read RJ (2020b) Density modification of cryo-EM maps. Acta Crystallogr D Struct Biol 76(Pt 10): 912–925

Tisza MJ, Zhao W, Fuentes JS, Prijic S, Chen X, Levental I, Chang JT (2016) Motility and stem cell properties induced by the epithelial-mesenchymal transition require destabilization of lipid rafts. Oncotarget 7(32): 51553–51568

Tong Y, Sun Y, Tian X, Zhou T, Wang H, Zhang T, Zhan R, Zhao L, Kuerban B, Li Z, Wang Q, Jin Y, Fan D, Guo X, Han H, Qin S, Chui D (2015) Phospholipid transfer protein (PLTP) deficiency accelerates memory dysfunction through altering amyloid precursor protein (APP) processing in a mouse model of Alzheimer's disease. Hum Mol Genet 24(19): 5388–5403

Tonggu L, Wang L (2018) Broken symmetry in the human BK channel. BioRxiv. https://doi.org/10.1101/494385

Tonggu L, Wang L (2022) Structure of the human BK ion channel in lipid environment. Membranes 12(8): 758. https://doi.org/10.3390/membranes12080758

Tran N-H, Carter SD, De Mazière A, Ashkenazi A, Klumperman J, Walter P, Jensen GJ (2021) The stress-sensing domain of activated IRE1α forms helical filaments in narrow ER

membrane tubes. Science 374(6563): 52–57
Turk M, Baumeister W (2020) The promise and the challenges of cryo-electron tomography. FEBS Lett 594(20): 3243–3261
Ueda Y, Levine BL, Huang ML, Freeman GJ, Nadler LM, June CH, Ward SG. (1995) Both CD28 ligands CD80 (B7-1) and CD86 (B7-2) activate phosphatidylinositol 3-kinase, and wortmannin reveals heterogeneity in the regulation of T cell IL-2 secretion. Int Immunol 7(6): 957–966
Ullrich J, Haueis L, Ohlhoff C, Zemella A, Kubick S, Stech M (2024) Solubilization of oligomeric cell-free synthesized proteins using SMA Copolymers. Methods Mol Biol 2762: 293–308
Unwin N (2020) Protein–lipid architecture of a cholinergic postsynaptic membrane. IUCrJ 7(5): 852–859
Unwin N (2022) Structure of a cholinergic cell membrane. Proc Natl Acad Sci USA 119(34): e2207641119. https://doi.org/10.1073/pnas.2207641119
Unwin N (2024) Influence of lipid bilayer on the structure of the muscle-type nicotinic acetylcholine receptor. Proc Natl Acad Sci USA 121(19): e2319913121. https://doi.org/10.1073/pnas.2319913121
Urzhumtsev AG, Urzhumtseva LM, Lunin VY (2022) Direct calculation of cryo-EM and crystallographic model maps for real-space refinement. Acta Crystallogr D Struct Biol 78(Pt 12): 1451–1468
Vidavsky N, Akiva A, Kaplan-Ashiri I, Rechav K, Addadi L, Weiner S, Schertel A (2016) Cryo-FIB-SEM serial milling and block face imaging: large volume structural analysis of biological tissues preserved close to their native state. J Struct Biol 196(3): 487–495
Wagner T, Lusnig L, Pospich S, Stabrin M, Schönfeld F, Raunser S (2020) Two particle-picking procedures for filamentous proteins: SPHIRE-crYOLO filament mode and SPHIRE-STRIPER. Acta Crystallogr D Struct Biol 76(Pt 7): 613–620
Wang B, Tieleman DP (2024) The structure, self-assembly and dynamics of lipid nanodiscs revealed by computational approaches. Biophys Chem 309: 107231. https://doi.org/10.1016/j.bpc.2024.107231
Wang C, Jiang W, Leitz J, Yang K, Esquivies L, Wang X, Shen X, Held R, Adams DJ, Basta T, Hampton L, Jian R, Jiang L, Stowell MHB, Baumeister W, Guo Q, Brunger AT (2024a) Structure and topography of the synaptic V-ATPase-synaptophysin complex. Nature 631(8022): 899–904
Wang L, Tonggu L (2015) Membrane protein reconstitution for functional and structural studies. Sci China Life Sci 58(1): 66–74
Wang L, Zhou H, Zhang M, Liu W, Deng T, Zhao Q, Li Y, Lei J, Li X, Xiao B (2019) Structure and mechanogating of the mammalian tactile channel PIEZO2. Nature 573(7773): 225–229
Wang X, Slater A, Lee SC, Harrison N, Pollock NL, Bakker SE, Navarro S, Nieswandt B, Dafforn TR, García Á, Watson SP, Tomlinson MG (2024b) Purification and characterisation of the platelet-activating GPVI/FcRγ complex in SMALPs. Arch Biochem Biophys 754: 109944. https://doi.org/10.1016/j.abb.2024.109944
Watson AJI, Bartesaghi A (2024) Advances in cryo-ET data processing: meeting the demands of visual proteomics. Curr Opin Struct Biol 87: 102861. https://doi.org/10.1016/j.sbi.2024.102861
Weis F, Hagen WJH (2020) Combining high throughput and high quality for cryo-electron microscopy data collection. Acta Crystallogr D Struct Biol 76(Pt 8): 724–728
Weissenberger G, Henderikx RJM, Peters PJ (2021) Understanding the invisible hands of sample preparation for cryo-EM. Nat Methods 18(5): 463–471
Westerlund AM, Fleetwood O, Pérez-Conesa S, Delemotte L (2020) Network analysis reveals how lipids and other cofactors influence membrane protein allostery. J Chem Phys 153(14): 141103. https://doi.org/10.1063/5.0020974
Wiedemann S, Heckel R (2024) A deep learning method for simultaneous denoising and missing wedge reconstruction in cryogenic electron tomography. Nat Commun 15(1): 8255. https://doi.org/10.1038/s41467-024-51438-y
Winter SL, Chlanda P (2021) Dual-axis Volta phase plate cryo-electron tomography of Ebola virus-like particles reveals actin-VP40 interactions. J Struct Biol 213(2): 107742. https://doi.org/10.1016/j.jsb.2021.107742
Wolff G, Limpens RWAL, Zevenhoven-Dobbe JC, Laugks U, Zheng S, de Jong AW M, Koning RI, Agard DA, Grünewald K, Koster AJ, Snijder EJ, Bárcena M (2020) A molecular pore spans the double membrane of the coronavirus replication organelle. Science 369(6509): 1395–1398
Wong F, Krishnan A, Zheng EJ, Stärk H, Manson AL, Earl AM, Jaakkola T, Collins JJ (2022) Benchmarking AlphaFold-enabled molecular docking predictions for antibiotic discovery. Mol Syst Biol 18(9): e11081. https://doi.org/10.15252/msb.202211081
Xu J, Liao C, Yin C-C, Li G, Zhu Y, Sun F (2024a) *In situ* structural insights into the excitation-contraction coupling mechanism of skeletal muscle. Sci Adv 10(12): eadl1126. https://doi.org/10.1126/sciadv.adl1126
Xu Y, Dang S (2022) Recent technical advances in sample preparation for single-particle cryo-EM. Front Mol Biosci 9: 892459. https://doi.org/10.3389/fmolb.2022.892459
Xu Z, Li H, Wan X, Fernández J-J, Sun F, Zhang F, Han R (2024b) Markerauto2: a fast and robust fully automatic fiducial marker-based tilt series alignment software for electron tomography. Structure 32(9): 1507–1518
Yamashita K, Palmer CM, Burnley T, Murshudov GN (2021) Cryo-EM single-particle structure refinement and map calculation using Servalcat. Acta Crystallogr D Struct Biol 77(Pt 10): 1282–1291
Yan X, Li S, Huang W, Wang H, Zhao T, Huang M, Zhou N, Shen Y, Li X. (2025) MPicker: visualizing and picking membrane proteins for cryo-electron tomography. Nat Commun 16: 472–13.
Yang J, Vrbovská V, Franke T, Sibert B, Larson M, Hall A, Rigort A, Mitchels J, Wright ER (2023) Integrated fluorescence microscopy (iFLM) for cryo-FIB-milling and *in-situ* cryo-ET. bioRxiv. https://doi.org/10.1101/2023.07.11.548578
Yang X, Lin C, Chen X, Li S, Li X, Xiao B (2022) Structure deformation and curvature sensing of PIEZO1 in lipid membranes. Nature 604(7905): 377–383
Yao X, Fan X, Yan N (2020) Cryo-EM analysis of a membrane protein embedded in the liposome. Proc Natl Acad Sci US A 117(31): 18497–18503
Yen HY, Hoi KK, Liko I, Hedger G, Horrell MR, Song W, Wu D, Heine P, Warne T, Lee Y, Carpenter B, Plückthun A, Tate CG, Sansom MSP, Robinson CV (2018) PtdIns(4, 5)P(2) stabilizes active states of GPCRs and enhances selectivity of G-protein coupling. Nature 559(7714): 423–427
Yokoyama H, Matsui I (2020) The lipid raft markers stomatin, prohibitin, flotillin, and HflK/C (SPFH)-domain proteins form an operon with NfeD proteins and function with apolar polyisoprenoid lipids. Crit Rev Microbiol 46(1): 38–48
You X, Zhang X, Cheng J, Xiao Y, Ma J, Sun S, Zhang X, Wang H-W, Sui S-F (2023) *In situ* structure of the red algal phycobilisome–PSII–PSI–LHC megacomplex. Nature 616(7955): 199–206
Yuan Z, Shen T, Xu S, Yu L, Pang B, Gan B, Feng Q, Ren R, Sun S (2024) AF2-mutation: adversarial sequence mutations against AlphaFold2 in protein tertiary structure prediction. Acta

Materia Medica 3(4): 462–476

ZachsT, Schertel A, Medeiros J, Weiss GL, Hugener J, Matos J, Pilhofer M (2020) Fully automated, sequential focused ion beam milling for cryo-electron tomography. eLife 9: e52286. https://doi.org/10.7554/eLife.52286

Zhang X, Zhang B, Freddolino PL, Zhang Y (2022) CR-I-TASSER: assemble protein structures from cryo-EM density maps using deep convolutional neural networks. Nat Methods 19(2): 195–204

Zhang Z, Huang L, Shulmeister VM, Chi Y-I, Kim KK, Hung L-W, Crofts AR, Berry EA, Kim S-H (1998) Electron transfer by domain movement in cytochrome bc1. Nature 392(6677): 677–684

Zhang Z, Li X, Yang F, Chen C, Liu P, Ren Y, Sun P, Wang Z, You Y, Zeng Y-X, Li X (2021) DHHC9-mediated GLUT1 S-palmitoylation promotes glioblastoma glycolysis and tumorigenesis. Nat Commun 12(1): 5872. https://doi.org/10.1038/s41467-021-26180-4

Zhao C (2024) Limitations in membrane protein structure determination by lipid nanodiscs. Trends Biochem Sci 49(6): 475–476

Zhao Q, Zhou H, Chi S, Wang Y, Wang J, Geng J, Wu K, Liu W, Zhang T, Dong M-Q, Wang J, Li X, Xiao B (2018) Structure and mechanogating mechanism of the Piezo1 channel. Nature 554(7693): 487–492

Zhao Y, Wang H, Wiesehoefer C, Shah NB, Reetz E, Hwang JY, Huang X, Wang T, Lishko PV, Davies KM, Wennemuth G, Nicastro D, Chung J-J (2022) 3D structure and *in situ* arrangements of CatSper channel in the sperm flagellum. Nat Commun, 13(1): 3439. https://doi.org/10.1038/s41467-022-31050-8

Zheng S, Wolff G, Greenan G, Chen Z, Faas FGA, Bárcena M, Koster AJ, Cheng Y, Agard DA (2022) AreTomo: an integrated software package for automated marker-free, motion-corrected cryo-electron tomographic alignment and reconstruction. J Struct Biol X 6: 100068. https://doi.org/10.1016/j.yjsbx.2022.100068

Zheng W, Chai P, Zhu J, Zhang K (2024) High-resolution *in situ* structures of mammalian respiratory supercomplexes. Nature 631(8019): 232–239

Zhou R, Zhang S, Nguyen HT, Ding H, Gaffney A, Kappes JC, Smith AB, Sodroski JG (2023) Conformations of human immunodeficiency virus envelope glycoproteins in detergents and styrene-maleic acid lipid particles. J Virol, 97(6): e0032723. https://doi.org/10.1128/jvi.00327-23

Zhu H, Li M, Zhao R, Li M, Chai Y, Zhu Z, Yang Y, Li W, Xie Z, Li X, Lei K, Li X, Ou G (2022) *In situ* structure of intestinal apical surface reveals nanobristles on microvilli. Proc Natl Acad Sci USA 119(24): e2122249119. https://doi.org/10.1073/pnas.2122249119

Zila V, Margiotta E, Turoňová B, Müller TG, Zimmerli CE, Mattei S, Allegretti M, Börner K, Rada J, Müller B, Lusic M, Kräusslich H-G, Beck M (2021) Cone-shaped HIV-1 capsids are transported through intact nuclear pores. Cell 184(4): 1032-1046. e18

Zivanov J, Otón J, Ke Z, von Kügelgen A, Pyle E, Qu K, Morado D, Castaño-Díez D, Zanetti G, Bharat TAM, Briggs JAG, Scheres SHW (2022) A Bayesian approach to single-particle electron cryo-tomography in RELION-4.0. eLife 11: e83724. doi: 10.7554/eLife.83724

Zuber B, Unwin N (2013) Structure and superorganization of acetylcholine receptor–rapsyn complexes. Proc Natl Acad Sci USA 110(26): 10622–10627